---

**Article:**
Zhang, J., Xu, H., Liu, W. orcid.org/0000-0003-2968-2888 et al. (2 more authors) (2021) Joint design of transmit weight sequence and receive filter for improved target information acquisition in high-resolution radar. IEEE Transactions on Geoscience and Remote Sensing, 60. 5104114. ISSN 0196-2892

https://doi.org/10.1109/tgrs.2021.3097115

---

# Joint Design of Transmit Weight Sequence and Receive Filter for Improved Target Information Acquisition in High-Resolution Radar

Jiawei Zhang, *Graduate Student Member, IEEE*, Huaping Xu, *Member, IEEE*, Wei Liu, *Senior Member, IEEE*, Chunsheng Li, and Yifan Chen, *Senior Member, IEEE*

***Abstract*— A joint design of the transmit weight sequence and receive filter is proposed to improve target information acquisition in high-resolution radar. First, using the criterion for target information acquisition maximization, the design is cast as a nonconvex fractional quadratically constrained quadratic problem (QCQP). Then, by employing a bivariate auxiliary function introduced in Dinkelbach's algorithm to decouple the fractional objective function, an algorithm with polynomial computational complexity is developed to solve the QCQP using a cyclic maximization procedure alternating between two semi-definite relaxation (SDR) problems. Through exploiting a suitable rank-one decomposition, it is verified that the optimal solution obtained from the alternative iterative process is also optimal to the original QCQP. Finally, numerical examples are presented to demonstrate the performance of the proposed design.**

***Index Terms*— Constrained optimization, high-resolution radar, information acquisition, receive filter, transmit weight.**

## I. Introduction

BY EMPLOYING a pulse-compression waveform to achieve both sufficient energy for target probing and the desired pulsewidth in time, high-resolution radar can effectively overcome the range-resolution dilemma [1]. Due to the ever-increasing resolution, even small and closely spaced targets become visible and identifiable [2], which allows for a large amount of target information to be extracted from the recorded data. Thus, it opens up a gateway to a number of advanced applications, including ship detection [3], aircraft classification [4], and vehicle recognition [5], [6]. Based on the Shannon information theory, the performance in these applications depends on the amount of information acquired about the observed target. As a result, improvement in the target information acquisition is of great significance.

Manuscript received March 23, 2021; revised May 24, 2021 and June 21, 2021; accepted July 4, 2021. This work was supported by the SAST Foundation of China under Grant SAST2019-026. *(Corresponding author: Huaping Xu.)*

Jiawei Zhang, Huaping Xu, and Chunsheng Li are with the School of Electronic and Information Engineering, Beihang University, Beijing 100191, China (e-mail: jwzhang@buaa.edu.cn; xuhuaping@buaa.edu.cn; lichunsheng@buaa.edu.cn).

Wei Liu is with the Department of Electronic and Electrical Engineering, The University of Sheffield, Sheffield S1 3JD, U.K. (e-mail: w.liu@sheffield.ac.uk).

Yifan Chen is with the School of Life Science and Technology, University of Electronic Science and Technology of China, Chengdu 610054, China, and also with the School of Engineering, University of Waikato, Hamilton 3240, New Zealand (e-mail: yifan.chen@uestc.edu.cn).

Under the point target assumption, one emphasis in the development of high-resolution radar is to increase the target detection performance, which relies on the signal-to-noise ratio (SNR) [7]. In order to achieve a sufficient SNR, the matched filter is always applied to suppress noise and maintain the useful signal. Moreover, the reflected waveform resulting from a point scatterer is compressed to realize the correlation function (CF) whose mainlobe resolution commensurates with what a very short pulse would have provided, along with the addition of range sidelobes [1]. As the CF shape determines the obtained SNR and the point-like target detection performance, it is expected that the CF should have a narrow mainlobe and much lower sidelobe levels [8], [9]. As a result, the design of waveform combined with the matched filter has been studied extensively to obtain the desirable shape of the mainlobe in terms of range resolution and peak SNR while suppressing the undesired sidelobes to avoid masking weak targets in the sidelobe of a closely spaced target. These results can be classified into two categories: frequency-modulated waveforms and phase codes.

Of the first category, the most prevalent pulse compression waveform employed in high-resolution radar is the linear frequency modulation (LFM) signal. A filtered LFM signal has the first sidelobe at a level of $-13$ dB to the peak of the mainlobe [10], [11]. If the continuous frequency range of the LFM signal is divided into a number of radio frequencies, it results in another high-resolution waveform: the stepped frequency waveform. It is a discrete frequency modulation technique for obtaining a large bandwidth and, thus, fine resolution [12]. To further reduce sidelobe levels, an amplitude taper is introduced using the window functions to weigh the LFM signal, such as the Taylor and Hamming windows [1]. Moreover, based on the LFM scheme, a variety of waveforms have been developed, which involves the nonlinear frequency modulation with a spectrum weighting function, leading to lower sidelobes compared to the classical LFM signal [11].

Another class of waveforms for high-resolution radar is phase codes, exemplified by the Frank, Barker, pseudorandom shift register coders, and the Lewis-Kretschmer P4 polyphase codes with a perfect periodic correlation [13]. In order to obtain a higher peak power after pulse compression, an optimization technique is employed in [14] to design phase codes focusing on the maximization of the peak-to-sidelobe ratio

of the CF. In [15], to synthesize phase sequences with good CF in terms of peak sidelobe level and integrated sidelobe level, a biobjective Pareto optimization is formulated, which is tackled through an iterative procedure. By using the same performance metric, binary sequences for multiple-input–multiple-output (MIMO) radar are designed in [16]. In [17], to improve target detection performance, a Pareto-optimal waveform design problem is formulated as maximizing the signal-to-interference-plus-noise ratio (SINR) subject to the peak-to-average power ratio.

From the target-detection point of view, the abovementioned works are effective to obtain high SNRs based on the point-like scattering model. However, the application of high-resolution radar includes not just point target detection but also classification, recognition, and tracking, where a higher information acquisition capability is always desired. The waveform design for maximizing SNR has been discussed widely in the past, but it is not clear whether maximizing SNR is equivalent to the maximization of target information acquisition. As early as 1964, Woodward [18] pointed out that pursuing SNR blindly can mislead radar design and data processing because there is no theory, which implies that maximizing SNR can ensure maximal information acquisition. A similar issue was also addressed by Bell [19]. From the practical applications of high-resolution radar, it is found that, to achieve high-precision target perception is still a difficult problem [20], [21]. Thus, the information acquisition capability of existing designs with SNR maximization needs further investigation and improvement, to meet the ever-increasing demand in practical applications.

The information acquisition capability of an active sensor can be improved by judiciously designing its transmit waveform [22], [23]. Bell's seminal work in [19] was the first to carry out research on waveform design based on the maximizing-target-information criterion (MTIC). With the mutual information (MI) between radar echo and target scattering signal as the objective function, the amplitude of waveform spectrum was obtained by the Lagrange multipliers method under an energy constraint. Subsequently, Leshem *et al.* [24] extended Bell's research to the case of multiple targets. The authors took the SNR and MI between echo and target scattering signals as the objective functions, respectively, to design the transmit waveform for clutter and noise suppression [25]. Experimental results demonstrated that the MI-based waveform was able to acquire a higher amount of information and achieve higher precision target recognition than the SNR-based one.

Bell's method has been extended to multiwaveform radar systems, such as MIMO radar and cognitive radar. Yang and Blum [26] considered the MI between echo and scattering signals as a criterion to design the MIMO radar waveform, which leads to the same result with the mean-square error criterion. The work in [27] followed the objective function in [26] to design the MI-based waveform with colored noise for MIMO radar and also presented a comparison between the MI criterion and the relative entropy criterion. Goodman *et al.* [28] introduced Bell's method to cognitive radar, where, with a feedback loop in the transceiver, the transmit waveform is adjusted continuously so that target information can be optimally acquired in real time. Other representative examples can also be found in [29]–[31], and all of them formulate the MI between the receive signal and target scattering as the objective function for optimization.

The abovementioned works aim to guarantee that the radar echo contains maximum information of the target, and subsequent target-perception experiments are also based on the echo. They consider the MI between radar echo and target scattering signal as the performance metric, and the optimization in the signal processing part of the radar receiver design is normally ignored. Although there are various studies to improve radar information acquisition by means of optimizing the transmit waveform, an optimal receive filter design based on the MI criterion has not been studied yet. The information acquisition of a high-resolution radar relies on both the transmit waveform and the receive filter, where the performance metric is the MI between the filtered signal (instead of the raw echo) and the target scattering characteristics. It is expected that both the transmit waveform and the receive filter are optimal in the MI sense to avoid performance degradation. Without designing a "matched" filter, it is not always possible to achieve both high resolution and optimal information acquisition at the same time.

In this article, a novel method is developed to improve information acquisition of high-resolution radar, via a joint design of the transmit weight sequence and receive filter under the MTIC. This design methodology can be useful for any existing high-resolution radar. The MI between the output signal of the receive filter and the target scattering characteristic function is considered as the objective function for the joint design. In addition to an energy condition, a similarity requirement is imposed on the weighted signal and receive filter to maintain high resolution. The design is then reformulated as a nonconvex fractional quadratically constrained quadratic problem (QCQP). An optimization procedure with a polynomial time complexity is introduced to sequentially improve the metric, by alternately solving two semidefinite relaxation (SDR) problems with a bivariate auxiliary function replacing the resultant fractional function. Following a rank-one decomposition stage, it is confirmed that the optimal solution obtained from the alternative iterative process is also optimal to the original QCQP. As demonstrated by computer simulations, with the optimal pair of transmit weight and receive filter, the newly designed high-resolution radar can achieve better performance than the classic one, in terms of both information acquisition and detection, with a similar resolution.

The rest of this article is organized as follows. Section II establishes the signal model and formulates the joint design of transmit weights and receive filters. In Section III, the optimization procedure is derived to tackle the resultant nonconvex fractional QCQP, followed by a discussion about the optimal solution, the convergence analysis, and the decomposition stage. Numerical results are provided in Section IV. Conclusions are drawn in Section V.

*Notations:* Throughout this article, matrices are denoted by bold uppercase letters and vectors by bold lowercase letters. $\mathbb{N}$, $\mathbb{C}$, and $\mathbb{C}^N$ represent the set of natural numbers, com-

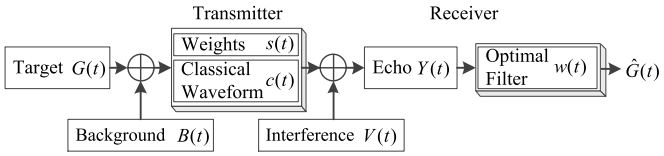


Fig. 1. Information acquisition model for the improved high-resolution radar.

plex numbers, and $N$-dimensional complex column vectors, respectively. The symbol $\bigcup$ denotes the union of two sets. The notation $\Re(\mathbf{A})$ denotes the range space of matrix $\mathbf{A}$, and $\mathrm{Re}(\cdot)$ is used for the real part of a complex number. The space of $N \times N$ complex Hermitian and nonzero semidefinite positive matrices are denoted by $\mathbb{H}^N$ and $\mathbb{H}_+^N$. $\mathbf{E}$ and $\mathbf{1}$ are the identity and all-one matrices. The superscripts $(\cdot)^T$, $(\cdot)^*$, and $(\cdot)^H$ denote the vector/matrix transpose, the complex conjugate, and the Hermitian transpose, respectively. $\otimes$ and $\odot$ represent the convolution operator and Hadamard (element-wide) product of vectors/matrices. The notation $\lambda_{\min}[\mathbf{A}]$ is the minimum eigenvalue of matrix $\mathbf{A}$. $|\cdot|$ stands for the modulus of a complex number. $\|\cdot\|$ and $\|\cdot\|_F$ denote the Euclidean norm and the Frobenius norm, respectively. The symbol $\mathrm{tr}[\cdot]$ and $\mathrm{rank}[\cdot]$ represent the trace and rank of a matrix. $\mathrm{E}[\cdot]$ represents the expectation operation. The notation $\mathbf{A} \succcurlyeq \mathbf{B}$ means that $\mathbf{A}-\mathbf{B}$ is positive semidefinite. $X \sim \mathcal{CN}(m, \sigma^2)$ indicates that random variable $X$ follows a circularly symmetric complex Gaussian distribution with mean $m$ and covariance $\sigma^2$. Finally, for any optimization problem $\mathcal{P}$, $\mathcal{V}(\mathcal{P})$ and $\mathcal{S}(\mathcal{P})$ represent its optimal value and the set of optimal solutions, respectively.

## II. Problem Formulation

In order to acquire target information, the classical high-resolution radar transmits a pulse signal periodically and employs the matched filter to achieve high resolution and SNR. Now, the signal is weighted by $s(t)$ in the time domain to form a new waveform, and the receive filter $w(t)$ is not the matched filter for SNR maximization as in the classical high-resolution radar but an optimal filter based on the MTIC. Following this working mechanism, the improved information acquisition process can be modeled by a memoryless channel with the information flow shown in Fig. 1.

The target scattering characteristic function $G(t)$ embedded in a uniform scene background $B(t)$ determines the information source and interacts with the new waveform $c(t)s(t)$ for spatial transmission. The modulated signal is then corrupted by signal-independent interference $V(t)$, including system noise, and/or intentional interference (jammer), and/or unintentional emissions from various telecommunication equipment [32]–[34]. After passing through the receive filter $w(t)$, direct estimation of target scattering characteristic $\hat{G}(t)$ is obtained as

$$\hat{G}(t) = \{[G(t) + B(t)] \otimes [c(t)s(t)] + V(t)\} \otimes w(t).$$

The existing waveform designs based on the MTIC involve maximizing the MI between radar echo $Y(t)$ and the target response $G(t)$ while ignoring the receive filter [19], [24]–[28]. Different from these works, here, the MI $I(G;\hat{G})$ between the filtered signal $\hat{G}(t)$ and $G(t)$ is considered such that the receive filter can be optimized together. The optimization problem of joint design for waveform weights and receive filter can be preliminarily expressed as

$$\max_{s(t),w(t)} I\big(G;\hat{G}\big). \tag{1}$$

From the central limit theorem, it is often assumed that radar signals follow a zero-mean complex Gaussian distribution [35]–[37]. All signals in Fig. 1 are random processes, and they follow the Gaussian distribution. Meanwhile, $G(t)$, $B(t)$, and $V(t)$ are statistically independent. At any given moment, the random variables corresponding to $G(t)$ and $\hat{G}(t)$ are represented by $G$ and $\hat{G}$, respectively, so that $G \sim \mathcal{CN}(0,\sigma_G^2)$ and $\hat{G} \sim \mathcal{CN}(0,\sigma_{\hat{G}}^2)$. $\sigma_G^2$ and $\sigma_{\hat{G}}^2$ denote the variance of $G(t)$ and $\hat{G}(t)$, respectively. Combining the definition of MI and the statistics of variables, $I(G;\hat{G})$ can be simplified into [38]

$$I\big(G;\hat{G}\big) = -\ln\Big(1 - \big|\rho\big(G;\hat{G}\big)\big|^2\Big)$$

where $\rho(G;\hat{G})$ is the Pearson correlation coefficient. The above formula shows that the MI is only related to $\rho(G;\hat{G})$ and is a monotonically increasing function of the modulus. Thus, the performance measure of information acquisition ability is equivalent to $\rho(G;\hat{G})$, which is defined as

$$\rho\big(G;\hat{G}\big) = \frac{\mathrm{E}\big[\hat{G}G^*\big]}{\sqrt{\mathrm{E}[GG^*]}\sqrt{\mathrm{E}\big[\hat{G}\hat{G}^*\big]}}. \tag{2}$$

To further derive $\rho(G;\hat{G})$, the discrete version of signals is considered. With $N \in \mathbb{N}$, use the notations $\mathbf{s}$, $\mathbf{c}$, $\mathbf{v}(\ell)$, $\mathbf{y}(\ell)$, and $\mathbf{w} \in \mathbb{C}^N$ to represent the weight sequence, the classic pulse-compression signal, interference, echo, and the optimal filter at a given time index $\ell$. The convolution operator can be implemented through a Toeplitz matrix [39], so the direct estimation of target scattering characteristic can be written as

$$\hat{G}(\ell) = \mathbf{w}^H\mathbf{y}(\ell) = \mathbf{w}^H[\mathcal{G}(\ell) + \mathcal{B}(\ell)](\mathbf{s}\odot\mathbf{c}) + \mathbf{w}^H\mathbf{v}(\ell)$$

where $\mathbf{s} = [s_0\ s_1\ \cdots\ s_{N-1}]^T$, $\mathbf{c} = [c_0\ c_1\ \cdots\ c_{N-1}]^T$, $\mathbf{v}(\ell) = [v(\ell)\ v(\ell+1)\ \cdots\ v(\ell+N-1)]^T$, and $\mathbf{w} = [w_0\ w_1\ \cdots\ w_{N-1}]^T$. $\mathcal{G}(\ell)$ is a Toeplitz matrix defined as

$$\mathcal{G}(\ell) = \begin{bmatrix} G(\ell) & G(\ell-1) & \cdots & G(\ell-N+1) \\ G(\ell+1) & G(\ell) & \ddots & \vdots \\ \vdots & \ddots & \ddots & G(\ell-1) \\ G(\ell+N-1) & \cdots & G(\ell+1) & G(\ell) \end{bmatrix}.$$

$\mathcal{B}(\ell)$ is also a Toeplitz matrix, similar to $\mathcal{G}(\ell)$. According to (2), with $\mathcal{Q}(\ell) = \mathcal{G}(\ell) + \mathcal{B}(\ell)$, $|\rho(G;\hat{G})|^2$ between the input and the output in Fig. 1 is derived as

$$\big|\rho\big(G;\hat{G}\big)\big|^2 = \frac{\mathbf{w}^H\mathbf{T}(\mathbf{s})\mathbf{w}}{\sigma_G^2\mathbf{w}^H[\mathbf{\Gamma}(\mathbf{s}) + \mathbf{R}_V]\mathbf{w}}$$

where

$$\begin{cases} \mathbf{T}(\mathbf{s}) = \mathbf{R}_G(\mathbf{s}\odot\mathbf{c})\big(\mathbf{c}^H\odot\mathbf{s}^H\big)\mathbf{R}_G^H \\ \mathbf{R}_G = \mathrm{E}[\mathcal{G}(\ell)G^*(\ell)] \end{cases} \tag{3}$$

and

$$\begin{cases} \mathbf{\Gamma}(\mathbf{s}) = \mathrm{E}\big[\mathcal{Q}(\ell)(\mathbf{s}\odot\mathbf{c})\big(\mathbf{c}^H\odot\mathbf{s}^H\big)\mathcal{Q}^H(\ell)\big] \\ \mathbf{R}_V = \mathrm{E}\big[\mathbf{v}(\ell)\mathbf{v}^H(\ell)\big]. \end{cases} \tag{4}$$

Then, the optimization problem (1) is equivalent to

$$\max_{\mathbf{s},\mathbf{w}} \ f(\mathbf{s},\mathbf{w}) = \frac{\mathbf{w}^H\mathbf{T}(\mathbf{s})\mathbf{w}}{\mathbf{w}^H[\mathbf{\Gamma}(\mathbf{s})+\mathbf{R}_V]\mathbf{w}}$$

where $\sigma_G^2$ is a constant and can be ignored. Because the unconstrained optimization can lead to signals with poor resolution, significant modulus variations, or even unrealizability, imposing some reasonable constraints on the shape of $\mathbf{s}$ and $\mathbf{w}$ is important and also beneficial to high-resolution radar [32]. In this context, in addition to the energy condition, a similarity constraint [40], [41] is imposed on the weight sequence

$$\|\mathbf{s}\odot\mathbf{c}-\mathbf{c}\|^2 \le \varepsilon_1 \tag{5}$$

where $\varepsilon_1$ is a parameter to determine the level of similarity required between the weighted waveform $\mathbf{s}\odot\mathbf{c}$ and the original waveform $\mathbf{c}$. With the similarity constraint in (5), the bandwidth of $\mathbf{s}\odot\mathbf{c}$ cannot decrease dramatically due to the large bandwidth of pulse compression signal $\mathbf{c}$, which helps maintain the high-resolution requirement.

Similar to (5), a receive filter with a large bandwidth is also needed to achieve a high resolution. To this end, a similarity constraint is introduced to $\mathbf{w}$, written as

$$\|\mathbf{w}-\mathbf{r}\|^2 \le \varepsilon_2$$

where $\mathbf{r}$ is a receive filter with a large bandwidth, such as the matched filter of $\mathbf{c}$. Finally, the problem of joint design of transmit weight sequence $\mathbf{s}$ and receive filter $\mathbf{w}$ under the energy, similarity, and spectrum constraints can be cast as the following optimization problem:

$$\mathcal{P}_{\mathbf{s},\mathbf{w}}\begin{cases}\max\limits_{\mathbf{s},\mathbf{w}} \ f(\mathbf{s},\mathbf{w})\\ \text{s.t.}\begin{cases}\|\mathbf{s}\odot\mathbf{c}\|^2 = E_s\\ \|\mathbf{s}\odot\mathbf{c}-\mathbf{c}\|^2 \le \varepsilon_1\\ \|\mathbf{w}\|^2 = E_w\\ \|\mathbf{w}-\mathbf{r}\|^2 \le \varepsilon_2\end{cases}\end{cases} \tag{6}$$

where $E_s$ and $E_w$ are energy of the weighted waveform and the receive filter, respectively.

## III. Solving the Optimization Problem

### A. Algorithmic Procedure

It can be seen that the resultant optimization (6) is a nonconvex fractional QCQP with multiple constraints, which is not easy to be tackled directly by existing methods [42], [43]. To solve the problem, the following procedure is adopted to find the desired solution from (6).

First, SDR can be introduced to deal with various constraints [44]. Let $\mathbf{X}=\mathbf{s}\mathbf{s}^H$ and $\mathbf{W}=\mathbf{w}\mathbf{w}^H$. We first transform the transmit weight vector optimization into the SDR representation

$$\mathcal{P}_{\mathbf{X},\mathbf{W}}\begin{cases}\max\limits_{\mathbf{X},\mathbf{W}} \ \bar{f}(\mathbf{X},\mathbf{W})\\ \text{s.t.}\begin{cases}\mathrm{tr}\big[\big(\mathbf{c}\mathbf{c}^H\odot\mathbf{E}\big)\mathbf{X}\big] = E_s\\ \mathrm{tr}\big[\big(\mathbf{c}\mathbf{c}^H\odot\big(\mathbf{c}\mathbf{c}^H\big)^*\big)\mathbf{X}\big] \ge \bar{\varepsilon}_1\\ \mathbf{X}\succcurlyeq 0\\ \mathrm{tr}[\mathbf{W}] = E_w\\ \mathrm{tr}\big[\mathbf{r}\mathbf{r}^H\mathbf{W}\big] \ge \bar{\varepsilon}_2\\ \mathbf{W}\succcurlyeq 0\end{cases}\end{cases} \tag{7}$$

where

$$\bar{f}(\mathbf{X},\mathbf{W}) = \frac{\mathrm{tr}\big[\bar{\mathbf{T}}(\mathbf{X})\mathbf{W}\big]}{\mathrm{tr}\big\{\big[\bar{\mathbf{\Gamma}}(\mathbf{X})+\mathbf{R}_V\big]\mathbf{W}\big\}} \tag{8}$$

with

$$\begin{aligned}\bar{\mathbf{T}}(\mathbf{X}) &= \mathbf{R}_G\big[\mathbf{X}\odot\big(\mathbf{c}\mathbf{c}^H\big)\big]\mathbf{R}_G^H\\ \bar{\mathbf{\Gamma}}(\mathbf{X}) &= [r_G(n_1-n_2)+r_B(n_1-n_2)]\\ &\quad\cdot\Bigg(\sum_{n_1=-N+1}^{N-1}\mathbf{J}_{n_1}\Bigg)\big[\mathbf{X}\odot\big(\mathbf{c}\mathbf{c}^H\big)\big]\Bigg(\sum_{n_2=-N+1}^{N-1}\mathbf{J}_{n_2}\Bigg)^H\\ \mathbf{J}_n(i,j) &= \begin{cases}1, & \text{if } i-j=n\\ 0, & \text{if } i-j\ne n\end{cases} \text{ and } \mathbf{R}_G = \sum_{n=-N+1}^{N-1} r_G(n)\mathbf{J}_n\end{aligned}$$

where $r_G$ and $r_B$ denote the autocorrelation functions of $G(t)$ and $B(t)$, respectively. The rank-one constraints of $\mathbf{X}$ and $\mathbf{W}$ are dropped since they are nonconvex [45], [46]. The associated proof is presented in Appendix A.

However, it is still not easy to solve $\mathcal{P}_{\mathbf{X},\mathbf{W}}$ as both numerator and denominator are functions of two variables to be optimized [47]. A bivariate auxiliary function introduced in Dinkelbach's algorithm is employed to decouple the numerator and the denominator [48], which is

$$\Psi\big(\mathbf{X},\mathbf{W};\tilde{\mathbf{X}},\tilde{\mathbf{W}}\big) = \mu(\mathbf{X},\mathbf{W}) - \eta(\mathbf{X},\mathbf{W})\bar{f}\big(\tilde{\mathbf{X}},\tilde{\mathbf{W}}\big)$$

with

$$\begin{cases}\bar{f}(\mathbf{X},\mathbf{W}) = \mu(\mathbf{X},\mathbf{W})/\eta(\mathbf{X},\mathbf{W})\\ \mu(\mathbf{X},\mathbf{W}) = \mathrm{tr}\big[\bar{\mathbf{T}}(\mathbf{X})\mathbf{W}\big]\\ \eta(\mathbf{X},\mathbf{W}) = \mathrm{tr}\big\{\big[\bar{\mathbf{\Gamma}}(\mathbf{X})+\mathbf{R}_V\big]\mathbf{W}\big\}.\end{cases} \tag{9}$$

$\Psi(\mathbf{X},\mathbf{W};\tilde{\mathbf{X}},\tilde{\mathbf{W}})$ is now considered as a new objective function of $\mathcal{P}_{\mathbf{X},\mathbf{W}}$.

Finally, based on a sequential optimization procedure, the optimization problem with the auxiliary function is divided into two problems corresponding to $\mathbf{X}$ and $\mathbf{W}$, respectively. They are alternately solved, which sequentially improves the value of $\bar{f}(\mathbf{X},\mathbf{W})$.

*1) Receive Filter Optimization:* At the $m$th step, given $\mathbf{X}=\tilde{\mathbf{X}}=\mathbf{X}^{(m-1)}$, $\mathbf{W}^{(m)}$ is expected to be solved first. Let $\tilde{\mathbf{W}}=\mathbf{W}^{(m-1)}$, and substituting it into the auxiliary function leads to the following problem:

$$\mathcal{P}_1\begin{cases}\max\limits_{\mathbf{W}} \ \Psi\big(\mathbf{X}^{(m-1)},\mathbf{W};\mathbf{X}^{(m-1)},\mathbf{W}^{(m-1)}\big)\\ \text{s.t.}\begin{cases}\mathrm{tr}[\mathbf{W}] = E_w\\ \mathrm{tr}[\mathbf{r}\mathbf{r}^H\mathbf{W}] \ge \bar{\varepsilon}_2\\ \mathbf{W}\succcurlyeq 0.\end{cases}\end{cases} \tag{10}$$

Using the toolbox in [49], an optimal solution $\mathbf{W}^{(m)}$ at the $m$th step will be obtained. It can be concluded that

$$\bar{f}\big(\mathbf{X}^{(m-1)},\mathbf{W}^{(m)}\big) \ge \bar{f}\big(\mathbf{X}^{(m-1)},\mathbf{W}^{(m-1)}\big). \tag{11}$$

A detailed proof is given in Appendix B.

*2) Transmit Weight Sequence Optimization:* Next, with a fixed $\mathbf{W}$ substituted into the auxiliary function, the optimization problem associated with $\mathbf{X}$ is established. Setting $\mathbf{W} = \tilde{\mathbf{W}} = \mathbf{W}^{(m)}$ and $\tilde{\mathbf{X}} = \mathbf{X}^{(m-1)}$, we have $\Psi(\mathbf{X}, \mathbf{W}^{(m)}; \mathbf{X}^{(m-1)}, \mathbf{W}^{(m)})$, which is not the standard form of SDR and, therefore, transformed into another equivalent version

$$\hat{\Psi}\left(\mathbf{X}, \mathbf{W}^{(m)}; \mathbf{X}^{(m-1)}, \mathbf{W}^{(m)}\right) = \hat{\mu}\left(\mathbf{X}, \mathbf{W}^{(m)}\right) - \hat{\eta}\left(\mathbf{X}, \mathbf{W}^{(m)}\right) \bar{f}\left(\mathbf{X}^{(m-1)}, \mathbf{W}^{(m)}\right) \tag{12}$$

where

$$\hat{\mu}\left(\mathbf{X}, \mathbf{W}^{(m)}\right) = \mathrm{tr}\left\{\left\{\left(\mathbf{c}\mathbf{c}^H\right)^* \odot \left[\mathbf{R}_G^H \mathbf{W}^{(m)} \mathbf{R}_G\right]\right\}\mathbf{X}\right\} \tag{13}$$

and

$$\hat{\eta}\left(\mathbf{X}, \mathbf{W}^{(m)}\right) = \mathrm{tr}\left\{\left[\left(\mathbf{c}\mathbf{c}^H\right)^* \odot \mathbf{\Lambda}\right]\mathbf{X}\right\} + \mathrm{tr}\left[\mathbf{R}_V \mathbf{W}^{(m)}\right] \tag{14}$$

with

$$\mathbf{\Lambda} = [r_G(n_1 - n_2) + r_B(n_1 - n_2)] \cdot \left(\sum_{n_2=-N+1}^{N-1} \mathbf{J}_{n_2}\right)^H \mathbf{W}^{(m)} \left(\sum_{n_1=-N+1}^{N-1} \mathbf{J}_{n_1}\right).$$

Through Appendix C, it can be confirmed that

$$\hat{\Psi}(\mathbf{X}, \mathbf{W}^{(m)}; \mathbf{X}^{(m-1)}, \mathbf{W}^{(m)}) = \Psi(\mathbf{X}, \mathbf{W}^{(m)}; \mathbf{X}^{(m-1)}, \mathbf{W}^{(m)}). \tag{15}$$

Combining the constraints of weight sequence, the optimization with respect to $\mathbf{X}$ is formed as

$$\mathcal{P}_2 \begin{cases} \max\limits_{\mathbf{X}} \ \hat{\Psi}\left(\mathbf{X}, \mathbf{W}^{(m)}; \mathbf{X}^{(m-1)}, \mathbf{W}^{(m)}\right) \\ \text{s.t.} \begin{cases} \mathrm{tr}\left[\left(\mathbf{c}\mathbf{c}^H \odot \mathbf{E}\right)\mathbf{X}\right] = E_s \\ \mathrm{tr}\left[\left(\mathbf{c}\mathbf{c}^H \odot \left(\mathbf{c}\mathbf{c}^H\right)^*\right)\mathbf{X}\right] \geq \bar{\varepsilon}_1 \\ \mathbf{X} \succcurlyeq 0. \end{cases} \end{cases} \tag{16}$$

Still employing the toolbox in [49], the optimal solution of $\mathcal{P}_2$ at the $m$th step is obtained. Assuming that an optimal solution of $\mathcal{P}_2$ at the $m$th step is obtained, then it can be proven that

$$\bar{f}\left(\mathbf{X}^{(m)}, \mathbf{W}^{(m)}\right) \geq \bar{f}\left(\mathbf{X}^{(m-1)}, \mathbf{W}^{(m)}\right). \tag{17}$$

The proof is similar with Appendix B. With (11), we finally obtain

$$\bar{f}\left(\mathbf{X}^{(m)}, \mathbf{W}^{(m)}\right) \geq \bar{f}\left(\mathbf{X}^{(m-1)}, \mathbf{W}^{(m)}\right) \geq \bar{f}\left(\mathbf{X}^{(m-1)}, \mathbf{W}^{(m-1)}\right). \tag{18}$$

Consequently, the proposed procedure with the auxiliary function is effective in obtaining a good solution to the optimization problem $\mathcal{P}_{\mathbf{X},\mathbf{W}}$ by alternately solving $\mathcal{P}_1$ and $\mathcal{P}_2$, as it can be verified that $\bar{f}(\mathbf{X}, \mathbf{W})$ is a monotonically increasing sequence during the iterative process. The implementation steps are summarized in Fig. 2.

In Fig. 2, $m$ demotes the iteration index. Starting from $m = 1$, $\mathbf{X} = \tilde{\mathbf{X}} = \mathbf{X}^{(m-1)}$, and $\tilde{\mathbf{W}} = \mathbf{W}^{(m-1)}$, the auxiliary function $\Psi(\mathbf{X}^{(m-1)}, \mathbf{W}; \mathbf{X}^{(m-1)}, \mathbf{W}^{(m-1)})$ associated with receive filter is generated. Then, $\mathbf{W}^{(m)}$ is obtained by solving the optimization problem $\mathcal{P}_1$ in (10). Using $\mathbf{W}^{(m)}$ to replace $\mathbf{W}^{(m-1)}$, the auxiliary function $\hat{\Psi}(\mathbf{X}, \mathbf{W}^{(m)}; \mathbf{X}^{(m-1)}, \mathbf{W}^{(m)})$ corresponding to weight sequence is established. After solving $\mathcal{P}_2$ in (16), we have $\mathbf{X}^{(m)}$. The iteration index is updated. After the stop condition is satisfied, $(\mathbf{X}^{(m)}, \mathbf{W}^{(m)})$ are then output as the optimized pair $(\mathbf{X}^{\dagger}, \mathbf{W}^{\dagger})$.

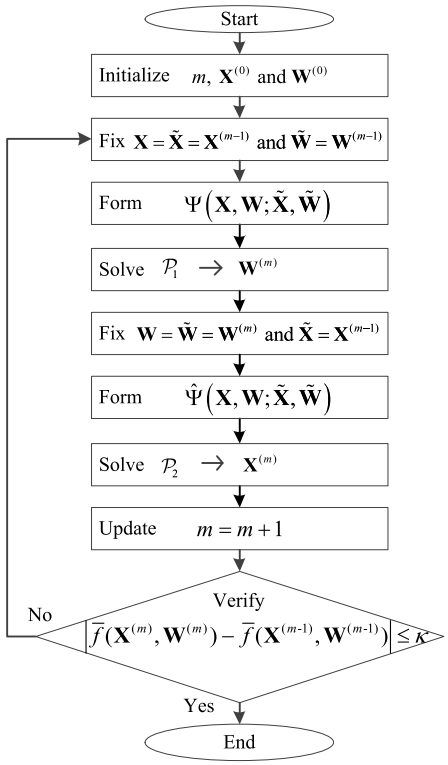


Fig. 2. Implementation of alternative iteration, where $\kappa$ is the maximum variation of the objective function. $|\bar{f}(\mathbf{X}^{(m)}, \mathbf{W}^{(m)}) - \bar{f}(\mathbf{X}^{(m-1)}, \mathbf{W}^{(m-1)})| \leq \kappa$ is considered as a stop condition.

### *B. Convergence Analysis*

The convergence of the objective function sequence can be demonstrated by showing that the objective function is monotonically increasing and converges to a finite value [45], [46]. By alternately solving $\mathcal{P}_1$ and $\mathcal{P}_2$, it has been verified that the objective function $\bar{f}(\mathbf{X}, \mathbf{W})$ is a monotonically increasing sequence, as shown in (18). Furthermore, it can be proved that $\bar{f}(\mathbf{X}, \mathbf{W})$ is upper bounded as follows.

Since $\mathrm{tr}[\mathbf{\Gamma}(\mathbf{s})\mathbf{W}] \geq 0$, from (8), we have

$$\bar{f}(\mathbf{X}, \mathbf{W}) \leq \frac{\mathrm{tr}[\mathbf{T}(\mathbf{s})\mathbf{W}]}{\mathrm{tr}[\mathbf{R}_V \mathbf{W}]}.$$

Considering $\mathrm{tr}[\mathbf{AB}] \leq \mathrm{tr}[\mathbf{A}]\mathrm{tr}[\mathbf{B}]$ [46] and $\mathrm{tr}[\mathbf{AB}] \geq \lambda_{\min}[\mathbf{A}]\mathrm{tr}[\mathbf{B}]$ [45], given $\mathbf{A}, \mathbf{B} \succcurlyeq \mathbf{0}$, there is

$$\bar{f}(\mathbf{X}, \mathbf{W}) \leq \frac{\mathrm{tr}[\mathbf{T}(\mathbf{s})]\mathrm{tr}[\mathbf{W}]}{\lambda_{\min}[\mathbf{R}_V]\mathrm{tr}[\mathbf{W}]}.$$

With (3), it follows that

$$\frac{\mathrm{tr}[\mathbf{T}(\mathbf{s})]\mathrm{tr}[\mathbf{W}]}{\lambda_{\min}[\mathbf{R}_V]\mathrm{tr}[\mathbf{W}]} = \frac{\mathrm{tr}\left[\mathbf{R}_G(\mathbf{s} \odot \mathbf{c})\left(\mathbf{c}^H \odot \mathbf{s}^H\right)\mathbf{R}_G^H\right]}{\lambda_{\min}[\mathbf{R}_V]}.$$

Finally, we have

$$\bar{f}(\mathbf{X},\mathbf{W}) \le \frac{E_s \mathrm{tr}\left[\mathbf{R}_G^H \mathbf{R}_G\right]}{\lambda_{\min}[\mathbf{R}_V]} = \frac{E_s \|\mathbf{R}_G\|_F^2}{\lambda_{\min}[\mathbf{R}_V]}.$$

Therefore, the above bounded objective function combined with the monotonic increasing property can ensure convergence.

### C. Discussion of the Optimal Solution

With (18), it can be proved that the optimal pair $(\mathbf{X}^\dagger, \mathbf{W}^\dagger)$ resulting from $\mathcal{P}_1$ and $\mathcal{P}_2$ are also optimal to $\mathcal{P}_{\mathbf{X},\mathbf{W}}$ when the alternate iteration is complete.

Suppose that, at the $m^*$th step, the optimal pair $\mathbf{X}^\dagger = \mathbf{X}^{(m^*)}$ and $\mathbf{W}^\dagger = \mathbf{W}^{(m^*)}$ are obtained. Thus, even with one more iteration, the value of $\bar{f}(\mathbf{X},\mathbf{W})$ remains unchanged, as it is a monotonically increasing function with iteration index shown in (18). Thus, we have

$$\begin{aligned}\bar{f}\left(\mathbf{X}^\dagger,\mathbf{W}^\dagger\right) &= \bar{f}\left(\mathbf{X}^{(m^*)},\mathbf{W}^{(m^*)}\right)\\ &= \bar{f}\left(\mathbf{X}^{(m^*)},\mathbf{W}^{(m^*+1)}\right) = \bar{f}\left(\mathbf{X}^{(m^*+1)},\mathbf{W}^{(m^*+1)}\right).\end{aligned} \tag{19}$$

Then, combing (12), it follows that the optimal value $\mathcal{V}(\mathcal{P}_2)$ of the problem $\mathcal{P}_2$ is

$$\begin{aligned}&\hat{\Psi}\left(\mathbf{X}^{(m^*+1)},\mathbf{W}^{(m^*+1)};\mathbf{X}^{(m^*)},\mathbf{W}^{(m^*+1)}\right)\\ &\quad= \hat{\mu}\left(\mathbf{X}^{(m^*+1)},\mathbf{W}^{(m^*+1)}\right) - \hat{\eta}\left(\mathbf{X}^{(m^*+1)},\mathbf{W}^{(m^*+1)}\right)\\ &\qquad\cdot \bar{f}\left(\mathbf{X}^{(m^*)},\mathbf{W}^{(m^*+1)}\right).\end{aligned}$$

With (19), we have

$$\begin{aligned}&\hat{\Psi}\left(\mathbf{X}^{(m^*+1)},\mathbf{W}^{(m^*+1)};\mathbf{X}^{(m^*)},\mathbf{W}^{(m^*+1)}\right)\\ &\quad= \hat{\Psi}\left(\mathbf{X}^{(m^*+1)},\mathbf{W}^{(m^*+1)};\mathbf{X}^{(m^*+1)},\mathbf{W}^{(m^*+1)}\right) = 0.\end{aligned} \tag{20}$$

Similarly, we have $\mathcal{V}(\mathcal{P}_1) = 0$ at the $m^*$th step. Next, we introduce a lemma:

*Lemma 1:* If $\mathcal{V}(\mathcal{P}_1) = \mathcal{V}(\mathcal{P}_2) = 0$ with obtained $\mathbf{W}^\dagger \in \mathcal{S}(\mathcal{P}_1)$ and $\mathbf{X}^\dagger \in \mathcal{S}(\mathcal{P}_2)$, then

$$\bar{f}(\mathbf{X}^\dagger,\mathbf{W}^\dagger) = \mathcal{V}(\mathcal{P}_{\mathbf{X},\mathbf{W}}). \tag{21}$$

Please refer to Appendix D for a detailed derivation. By using the above lemma, it can be proved that the waveform–filter pair $(\mathbf{X}^\dagger,\mathbf{W}^\dagger)$ resulting from the alternative iterations are also optimal to the problem $\mathcal{P}_{\mathbf{X},\mathbf{W}}$.

### D. Decomposition Stage

The optimization process sequentially converges to an optimized pair $(\mathbf{X}^\dagger,\mathbf{W}^\dagger)$, and then, a rank-one decomposition is employed to derive the optimal transmit weight vector $\mathbf{s}^\dagger$ and $\mathbf{w}^\dagger$ from the obtained $\mathbf{X}^\dagger$ and $\mathbf{W}^\dagger$, respectively. An effective method to construct a rank-one solution is given by a recent rank-one matrix decomposition theorem [50, Th. 2.2], which is cited as the following lemma.

*Lemma 2:* With $N \ge 3$, suppose that $\mathbf{A}_1, \mathbf{A}_2, \mathbf{A}_3 \in \mathbb{H}^N$ and $\mathbf{X} \in \mathbb{H}_+^N$ involving the rank-one decomposition. Let $\mathrm{rank}[\mathbf{X}] = r$; then, the following holds.

1) If $r \ge 3$, one can find in polynomial time, a nonzero vector in $\mathbf{s} \in \Re(\mathbf{X})$ such that
$$\mathbf{s}^H \mathbf{A}_i \mathbf{s} = \mathrm{tr}[\mathbf{A}_i \mathbf{X}], \quad i = 1,2,3$$
with $\mathbf{X} - (1/r)\mathbf{s}\mathbf{s}^H \succcurlyeq \mathbf{0}$ and $\mathrm{rank}[\mathbf{X} - (1/r)\mathbf{s}\mathbf{s}^H] \le r-1$.
2) If $r = 2$, for any $\mathbf{z} \in \mathbb{C}^N$ not in the range space of $\mathbf{X}$, there exists a vector $\mathbf{s}$ belonging to the linear subspace spanned by $[\mathbf{z} \bigcup \Re(\mathbf{X})]$ such that
$$\mathbf{s}^H \mathbf{A}_i \mathbf{s} = \mathrm{tr}[\mathbf{A}_i \mathbf{X}], \quad i = 1,2,3$$
with $\mathbf{X} + \mathbf{z}\mathbf{z}^H - (1/r)\mathbf{s}\mathbf{s}^H \succcurlyeq \mathbf{0}$ and $\mathrm{rank}[\mathbf{X} + \mathbf{z}\mathbf{z}^H - (1/r)\mathbf{s}\mathbf{s}^H] \le 2$.
3) If $r = 1$, it can be tackled by eigendecomposition directly.

Through Lemma 2, $\mathbf{X}^\dagger$ and $\mathbf{W}^\dagger$ can be decomposed, which results in $\mathbf{s}^\dagger$ and $\mathbf{w}^\dagger$. Taking $\mathbf{X}^\dagger$ as an example, it is expected that $\mathbf{s}^\dagger(\mathbf{s}^\dagger)^H$ can reach the optimal value of the objective function and satisfy all constraints of $\mathcal{P}_2$ such that

$$\begin{cases}\hat{\Psi}\left(\mathbf{X}^\dagger,\mathbf{W}^{(m)};\mathbf{X}^{(m-1)},\mathbf{W}^{(m)}\right)\\ = \hat{\Psi}\left(\mathbf{s}^\dagger(\mathbf{s}^\dagger)^H,\mathbf{W}^{(m)};\mathbf{X}^{(m-1)},\mathbf{W}^{(m)}\right)\\ \mathrm{tr}\left[\mathbf{B}\mathbf{X}^\dagger\right] = \mathrm{tr}\left[\mathbf{B}\mathbf{s}^\dagger(\mathbf{s}^\dagger)^H\right] = (\mathbf{s}^\dagger)^H\mathbf{B}\mathbf{s}^\dagger = E_s\\ \mathrm{tr}\left[\mathbf{C}\mathbf{X}^\dagger\right] = \mathrm{tr}\left[\mathbf{C}\mathbf{s}^\dagger(\mathbf{s}^\dagger)^H\right] = (\mathbf{s}^\dagger)^H\mathbf{C}\mathbf{s}^\dagger \ge \bar{\varepsilon}_1\end{cases}$$

where $\mathbf{B} = \mathbf{c}\mathbf{c} \odot \mathbf{E}$ and $\mathbf{C} = \mathbf{c}\mathbf{c}^H \odot (\mathbf{c}\mathbf{c}^H)^*$. According to Lemma 2, $\mathbf{A}_1$, $\mathbf{A}_2$, and $\mathbf{A}_3$ for $\mathbf{s}^\dagger$ are given as $\mathbf{A}_1 = \mathbf{B}$, $\mathbf{A}_2 = \mathbf{C}$, and $\mathbf{A}_3 = \mathbf{P}_1 - \bar{f}(\mathbf{X}^\dagger,\mathbf{W}^\dagger)\mathbf{P}_2$, where

$$\begin{cases}\mathbf{P}_1 = \left(\mathbf{c}\mathbf{c}^H\right)^* \odot \left(\mathbf{R}_G^H \mathbf{W}^\dagger \mathbf{R}_G\right)\\ \mathbf{P}_2 = \left(\mathbf{c}\mathbf{c}^H\right)^* \odot \mathbf{\Lambda}.\end{cases}$$

A more detailed implementation procedure of rank-one decomposition is available in [50]. Suppose that $\mathbf{s}^\dagger$ is the result of rank-one decomposition by applying Lemma 2; then, we have

$$(\mathbf{s}^\dagger)^H \mathbf{A}_3 \mathbf{s}^\dagger = \mathrm{tr}[\mathbf{A}_3 \mathbf{X}^\dagger].$$

With (20), it follows that

$$(\mathbf{s}^\dagger)^H \mathbf{P}_1 \mathbf{s}^\dagger - \bar{f}(\mathbf{X}^\dagger,\mathbf{W}^\dagger)\left[(\mathbf{s}^\dagger)^H \mathbf{P}_2 \mathbf{s}^\dagger + c_w\right] = 0$$

where $c_w = \mathrm{tr}[\mathbf{R}_V \mathbf{W}^\dagger]$. Considering the objective function $f(\mathbf{s},\mathbf{w})$ of the original problem $\mathcal{P}_{\mathbf{s},\mathbf{w}}$ in (6), for any $\mathbf{s} = \mathbf{s}^\dagger$, there always exists

$$(\mathbf{s}^\dagger)^H \mathbf{P}_1 \mathbf{s}^\dagger - f(\mathbf{s}^\dagger,\mathbf{w}^\dagger)\left[(\mathbf{s}^\dagger)^H \mathbf{P}_2 \mathbf{s}^\dagger + c_w\right] = 0.$$

Since $(\mathbf{s}^\dagger)^H \mathbf{P}_2 \mathbf{s}^\dagger + c_w > 0$, we finally obtain

$$f(\mathbf{s}^\dagger,\mathbf{w}^\dagger) = \bar{f}(\mathbf{X}^\dagger,\mathbf{W}^\dagger).$$

Thus, the optimal solution of $\mathcal{P}_{\mathbf{X},\mathbf{W}}$ is also optimal to $\mathcal{P}_{\mathbf{s},\mathbf{w}}$, and the SDR in (16) is tight, by resorting to Lemma 2. With (21), there will be

$$\bar{f}(\mathbf{X}^\dagger,\mathbf{W}^\dagger) = \mathcal{V}(\mathcal{P}_{\mathbf{X},\mathbf{W}}) = \mathcal{V}(\mathcal{P}_{\mathbf{s},\mathbf{w}})$$

when both the iteration process and rank-one decomposition are completed. Consequently, the solving method by a cyclic maximization procedure alternating between the

two SDR problems, followed by the rank-one decomposition stage, can find the optimal solution of the original problem $\mathcal{P}_{\mathbf{s},\mathbf{w}}$.

The overall computational complexity of the algorithm includes the computation of alternating iteration and rank-one decomposition. The former mainly depends on solving the two SDRs, which is of $\mathcal{O}(N^{3.5}\log(1/\xi))$, where $\xi > 0$ is the required solution accuracy parameter. The latter is implemented with a complexity of $\mathcal{O}(N^3)$ [50]. In summary, the original QCQP can be tackled by the solving method involving a polynomial computational complexity.

## IV. Numerical Examples

In this section, numerical examples are provided to verify the effectiveness of the proposed method for joint optimization of the weight sequence and receive filter. The proposed method can enhance the target information acquisition ability of any high-resolution radar. Without loss of generality, we perform experiments based on two high-resolution radars: the LFM radar with LFM signal and the P4 radar with P4 polyphase codes.

### A. Theoretical Analysis Verification

*1) Convergence of the Solving Method:* For both the LFM radar and P4 radar, we set similar parameters,[1] and perform the same experiments subsequently. The minimum variation of objective function is set to $\kappa = 10^{-3}$. Suppose that $V(t)$ and $B(t)$ hold a constant power spectrum density (PSD) over the system frequency band, and their variance depends on the value of the signal-to-interference ratio (SIR[2]) and the signal-to-clutter ratio (SCR), which will be given in the following. Referring to the target scattering PSD in [25], $r_G$ is then obtained by the inverse Fourier transform of its PSD. Similarly, $r_B$ and $\mathbf{R}_V$ are generated according to their PSDs. Initializing $\mathbf{X}^{(0)}$ and $\mathbf{W}^{(0)}$ with $\mathbf{1}$ and $\mathbf{c}\mathbf{c}^H$, respectively, the obtained pair $(\mathbf{X}^\dagger, \mathbf{W}^\dagger)$ at the iteration stage is output for these two radars when the stop criterion is satisfied.

In order to verify the convergence of the proposed method, the change of objective function $\bar{f}(\mathbf{X},\mathbf{W})$ of $\mathcal{P}_{\mathbf{X},\mathbf{W}}$ is presented with respect to the iteration number, as shown in Fig. 3, for different values of the similarity parameters $\varepsilon_1$ and $\varepsilon_2$.

It can be seen that $\bar{f}(\mathbf{X},\mathbf{W})$ of both radars increases with the number of iterations. As derived in (18), the objective function of $\mathcal{P}_{\mathbf{X},\mathbf{W}}$ keeps increasing monotonically with the alternate iterative process proceeding. Moreover, the algorithm converges rapidly, which is demonstrated by $\bar{f}(\mathbf{X},\mathbf{W})$ reaching a relatively stable state only after three or four iterations.

Compared to the red line in Fig. 3(a) corresponding to $\varepsilon_1 = 1.0$, increasing $\varepsilon_1$ from 1.0 to $\infty$ leads to substantial improvement of $\bar{f}(\mathbf{X},\mathbf{W})$. As expected, other figures also show a similar pattern. In summary, the algorithm is effective and efficient in tackling the original SDR problem $\mathcal{P}_{\mathbf{X},\mathbf{W}}$.

[1]Set system sampling frequency $f_s = 110$ MHz for both radars and the number of samples $N = 40$ and $E_s = E_w = E_c = N$.

[2]SIR = $\mathrm{E}[|G(t)|^2]/\mathrm{E}[|V(t)|^2]$ and SCR = $\mathrm{E}[|G(t)|^2]/\mathrm{E}[|B(t)|^2]$.

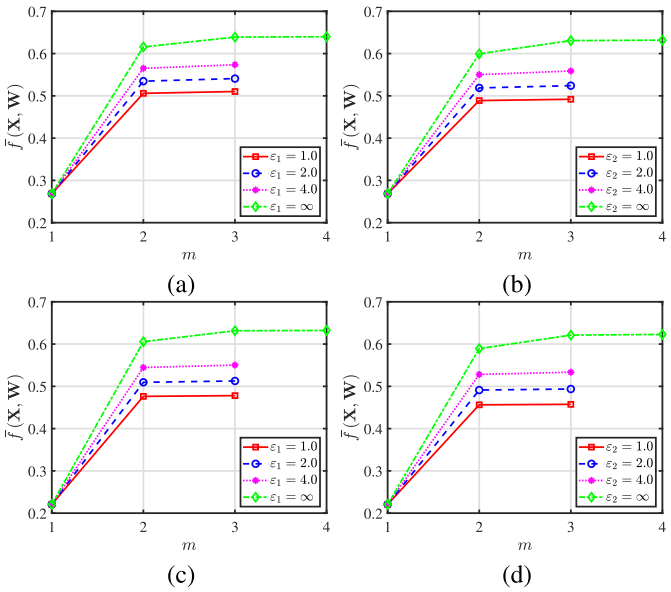


Fig. 3. Objective functions for different feasible regions: (a) $\bar{f}(\mathbf{X},\mathbf{W})$ corresponding to the LFM radar for a different $\varepsilon_1$ with $\varepsilon_2 = 1.5$, (b) $\bar{f}(\mathbf{X},\mathbf{W})$ corresponding to the LFM radar for a different $\varepsilon_2$ with $\varepsilon_1 = 1.0$, (c) $\bar{f}(\mathbf{X},\mathbf{W})$ corresponding to the P4 radar for a different $\varepsilon_1$ with $\varepsilon_2 = 1.5$, and (d) $\bar{f}(\mathbf{X},\mathbf{W})$ corresponding to the P4 radar for a different $\varepsilon_2$ with $\varepsilon_1 = 1.0$. Here, set SIR $= -20$ dB and SCR $= 0$ dB, and the symbol $\infty$ means that the associated constrains is relaxed.

*2) High-Resolution Requirement:* As mentioned above, the similarity constraint is imposed on both the weight sequence and receive filter, in order to maintain its resolution by keeping a larger bandwidth. To investigate the effectiveness of this scheme, the optimal weight sequence $\mathbf{s}^\dagger$ and the receive filter $\mathbf{w}^\dagger$ are synthesized at the decomposition stage, based on the results obtained in Fig. 3. Then, we plot the CFs of $\mathbf{s}^\dagger \odot \mathbf{c}$ and $\mathbf{w}^\dagger$ versus different similarity constraint parameters, as shown in Figs. 4 and 5.

It is easy to notice that the resultant mainlobe width of CFs depends on the value of similarity constraint parameters $\varepsilon_1$ and $\varepsilon_2$, no matter which radar it is. More precisely, when $\varepsilon_1$ and $\varepsilon_2$ both have relatively small values, for example, 1.0 and 1.5, the mainlobe of CF is obviously narrower than the case of $\varepsilon_1 = \infty$ and $\varepsilon_2 = \infty$. Moreover, Figs. 4 and 5 have shown that the similarity constraint is needed for both transmit weight sequence and receive filter, as both $\varepsilon_1 = \infty$ and $\varepsilon_2 = \infty$ result in a poor resolution. Therefore, the similarity constraints imposed on the weights and receive filter are effective for guaranteeing that the resolution cannot be reduced too much compared to the original radar systems, and the desired resolution can be obtained by adjusting $\varepsilon_1$ and $\varepsilon_2$.

### B. Performance Assessment

*1) Information Acquisition:* Referring to Fig. 3, the optimal weight sequence $\mathbf{s}^\dagger$ and the receive filter $\mathbf{w}^\dagger$ with different $\varepsilon_1$ and $\varepsilon_2$ are then synthesized. We evaluate the information acquisition capability of the proposed scheme, compared with the classical LFM radar and P4 radar, by plotting $|\rho(G;\hat{G})|^2$ versus different SIRs and SCRs, as shown in Fig. 6.

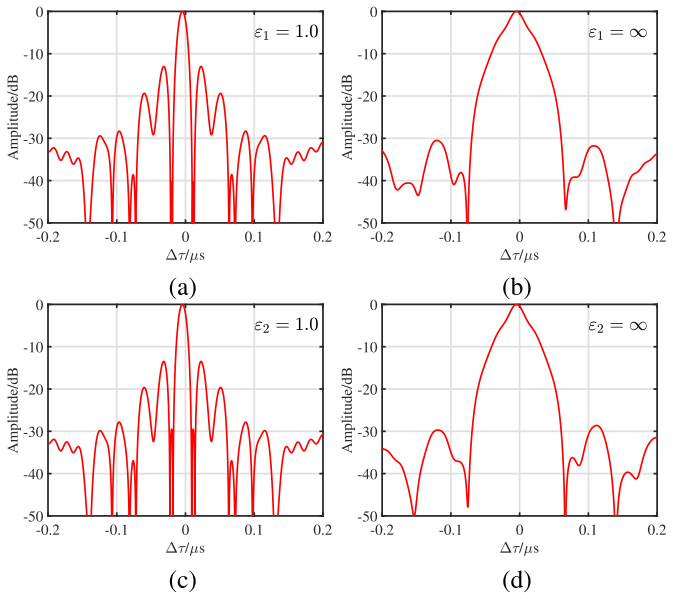


Fig. 4. CFs of the improved LFM radar for different feasible regions: (a) CF of $\varepsilon_1 = 1.0$ with $\varepsilon_2 = 1.5$, (b) CF of $\varepsilon_1 = \infty$ with $\varepsilon_2 = 1.5$, (c) CF of $\varepsilon_2 = 1.0$ with $\varepsilon_1 = 1.0$, and (d) CF of $\varepsilon_2 = \infty$ with $\varepsilon_1 = 1.0$.

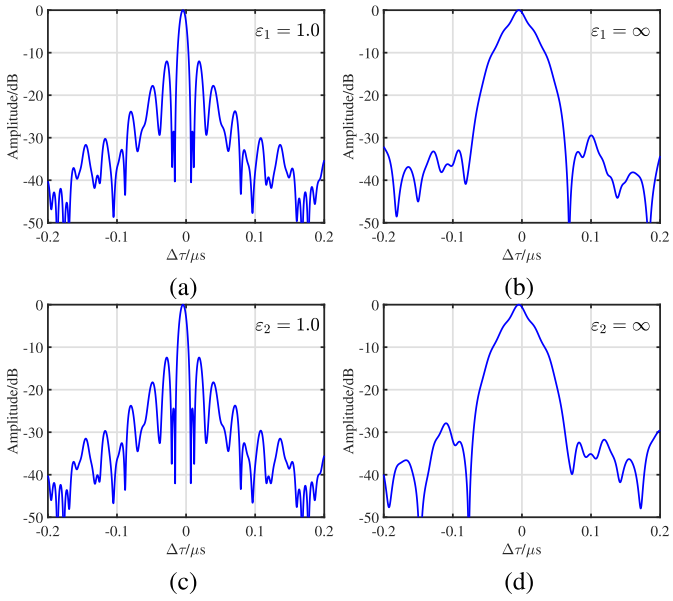


Fig. 5. CFs of the improved P4 radar for different feasible regions: (a) CF of $\varepsilon_1 = 1.0$ with $\varepsilon_2 = 1.5$, (b) CF of $\varepsilon_1 = \infty$ with $\varepsilon_2 = 1.5$, (c) CF of $\varepsilon_2 = 1.0$ with $\varepsilon_1 = 1.0$, and (d) CF of $\varepsilon_2 = \infty$ with $\varepsilon_1 = 1.0$.

Meanwhile, we also consider a widely discussed MI-based waveform design scheme, which is called the "water-filling" method [19], [25], as a benchmark for comparison. Since the associated receive part has always been ignored in such works, the traditional matched filter is assumed to be the receive filter.

It can be found that the improved radars with $\mathbf{s}^{\dagger} \odot \mathbf{c}$ and $\mathbf{w}^{\dagger}$ have achieved a better result than the classical systems and the water-filling method, which is demonstrated by the maximum $|\rho(G;\hat{G})|^2$ over the most considered SIR or SCR range. By contrast, the maximum gap of $|\rho(G;\hat{G})|^2$ between the improved LFM radar and the classical one is about 0.28,

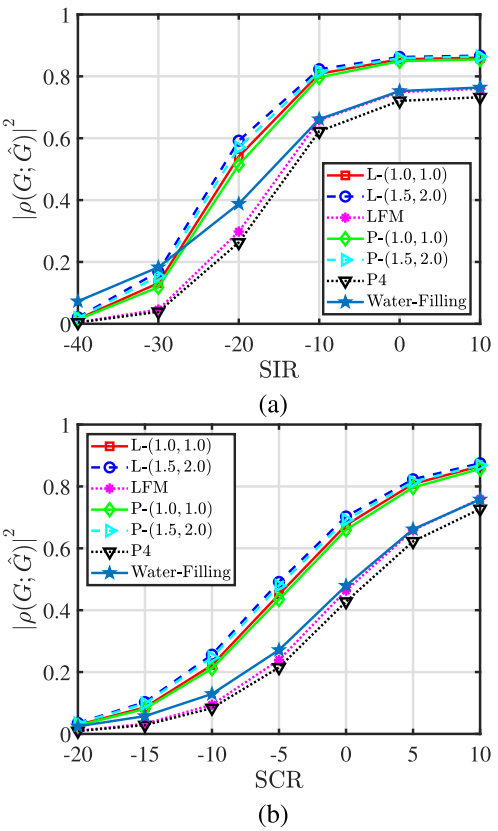


Fig. 6. Information acquisition comparisons: (a) $|\rho(G;\hat{G})|^2$ versus different SIRs with fixed SCR = 5 dB and (b) $|\rho(G;\hat{G})|^2$ versus different SCRs with fixed SIR = $-10$ dB, where the legend "L-$(a, b)$" in each figure indicates the improved LFM radar with $\varepsilon_1 = a$ and $\varepsilon_2 = b$. Similarly, the symbol "P-" demotes the improved P4 radar, and "LFM" and "P4" represent the classical LFM radar and the P4 radar, respectively.

with a feasible region of $\varepsilon_1 = 1.5$ and $\varepsilon_2 = 2.0$ in Fig. 6(a). The obvious gap can also be seen over different SCRs in Fig. 6(b). Increasing $\varepsilon_1$ and $\varepsilon_2$ results in an improvement of $|\rho(G;\hat{G})|^2$ for both types of radar, which is consistent with Fig. 3.

Moreover, compared with the recent water-filling method, the proposed scheme also shows higher information acquisition capability, except for the cases with extremely low SIRs. The reason is that the water-filling method only focuses on the MI between the echo and target scattering signal. Although both the water-filling method and the proposed scheme consider the MI as the performance metric, their objective functions are totally different. As mentioned above, the receive part in the water-filling case is ignored. Even using the matched filter as the receive filter, it is still not an optimal scheme for the joint waveform–filter design maximizing the MI between the signal after being filtered and the target scattering characteristics. Furthermore, Fig. 6(b) indicates that the water-filling method has lower $|\rho(G;\hat{G})|^2$ over all considered SCR ranges, which presents a different pattern to Fig. 6(a). It can be explained by the principle of the matched filter, as the matched filter is mainly derived for signal-independent interference (including noise) suppression based on the SIR criterion but not for any signal-dependent interference. Thus, when the white noise $N(t)$ is really significant with extremely

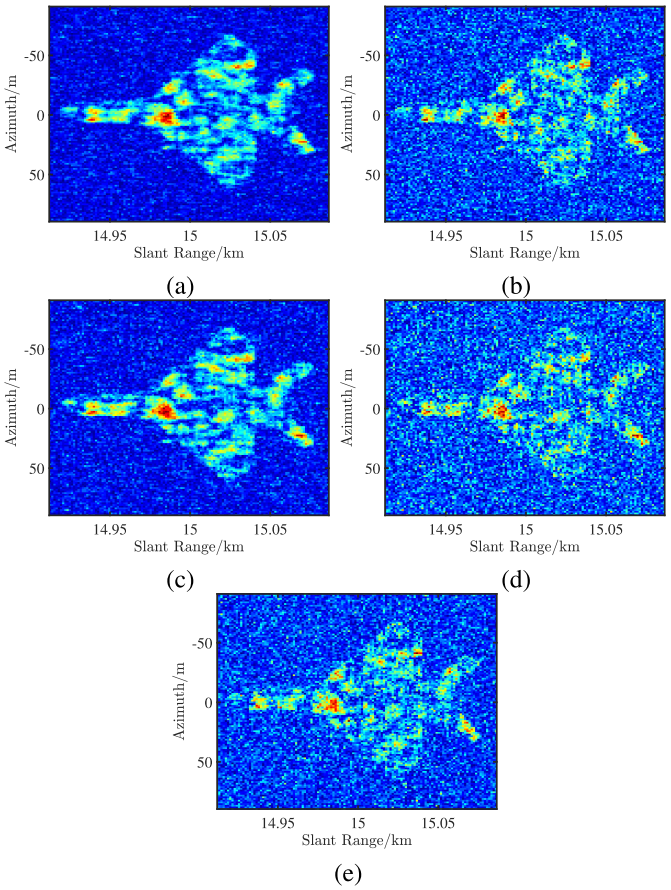


Fig. 7. SAR images with different waveforms: (a) SAR image of the weighted LFM signal, (b) SAR image of the classical LFM signal, (c) SAR image of the weighted P4 sequence, (d) SAR image of the classical P4 sequence, and (e) SAR image of the water-filling waveform with its matched filter, where $\varepsilon_1 = 1.5$ and $\varepsilon_2 = 2.0$ are fixed. SIR $= -10$ dB, and SCR $= 5$ dB.

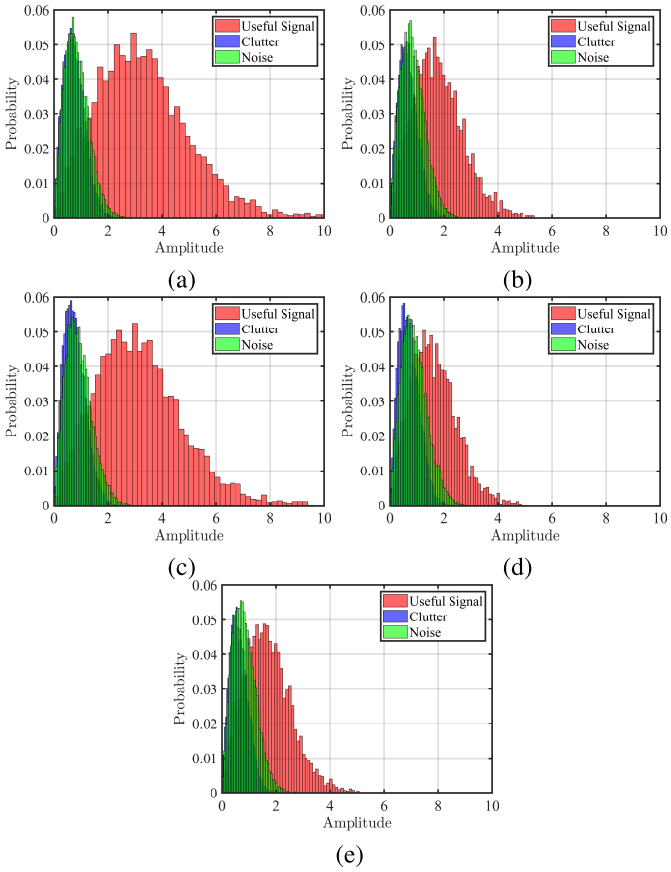


Fig. 8. Probability histogram of SAR images: (a) result of the proposed pair to the LFM signal, (b) result of the classical pair to the LFM signal, (c) result of the proposed pair to the P4 sequence, (d) result of the classical pair to the P4 sequence, and (e) result of the water-filling waveform and the matched filter.

low SIRs, the matched filter becomes a near-optimal filter. Meanwhile, it should be noted that the water-filling scheme only has an energy condition, which indicates a larger feasible set of optimization problems than the proposed scheme. Thus, the water-filling case can obtain relatively high $|\rho(G;\hat{G})|^2$ over the extremely low SIR range.

*2) Target Detection:* The information acquisition performance can be further measured in terms of target detection capability [31], [51]. In this part, we evaluate the performance of different radar systems with respect to their detection capabilities. To this end, synthetic aperture radar (SAR) is introduced to support the experiment. The range profile of SAR is equivalent to a pulse compression waveform processed by its matched filter, which is similar to the classical high-resolution radar with the 1-D signal model. Therefore, the SAR echo can be viewed as a set of receive signals with different time delays, and performance comparisons can also be based on the SAR with the abovementioned waveforms and range filters.

The radar scene is simulated by placing an aircraft at a fixed location on grass, which is flat and uniform. It is assumed that there is an SAR system with five waveforms, and they are the weighted LFM signal and P4 sequence, the classical versions, and the water-filling waveform. Meanwhile, suppose that all waveforms are independent of each other during the observing process, and we use SAR with these five waveforms to illuminate the scene and store the associated receive signals for echo generation. Then, a tailor-made imaging algorithm for these waveform–filter pairs is applied to provide SAR images, as shown in Fig. 7. Based on the range-Doppler algorithm, the SAR imaging process can be summarized as three steps: range filtering, range migration correction, and azimuth filtering. Here, we only change the first step by using the considered waveform–filter pairs to achieve range filtering.

It can be seen that the SAR images corresponding to the proposed method have the best result. Specifically, the one with the pair of weighted LFM waveform and filter shows more explicit aircraft contour and shape than the classical one. The results of P4 also reveal a similar pattern. As for the water-filling SAR image, the pixels of the background area are relatively bright and messy, which has lower image quality than the proposed scheme.

To further compare their ability in discriminating between the useful part and background clutter, the probability histogram of each signal component of SAR images in Fig. 7 is presented as follows.

Fig. 8 indicates that the proposed scheme associated with these two weighted waveforms has achieved a better

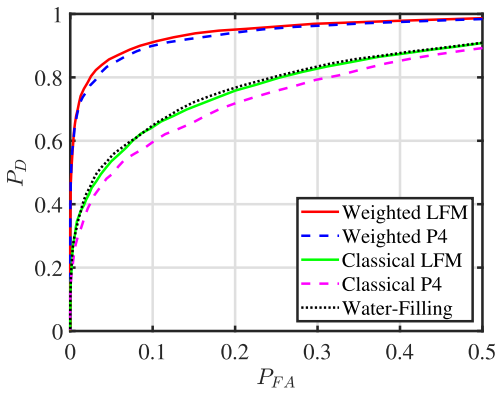


Fig. 9. Detection probability and false alarm probability for different waveforms.

TABLE I
RESOLUTION INDEX

| Index / waveform | 3dB Mainlobe Width ($\mu$s) |
|---|---|
| Weighted LFM | 0.0107 |
| Classical LFM | 0.0090 |
| Weighted P4 | 0.0098 |
| Classical P4 | 0.0082 |
| Water-Filling | 0.0082 |

distinguishing result, as most proportions of the useful signal are distributed in the amplitude range where both clutter and noise barely exist. For the case of the water-filling method, there is a significant aliasing effect for the interval from 0 to 2 in Fig. 8(e), resulting in relatively poor discrimination performance.

Based on Figs. 7 and 8, the detection probability $P_D$ and the false alarm probability $P_{\text{FA}}$ of these five waveforms are presented in Fig. 9.

It is clear that the detection accuracy of the proposed schemes is higher than that of the classical waveforms and the water-filling method, which further demonstrates that the joint design can help the classical waveforms acquire more target information. The aircraft can be discriminated very well by the proposed joint design with $P_{\text{FA}} = 0.1$. By comparison, the same level of $P_D$ can only be achieved in the case of $P_{\text{FA}}$ higher than 0.5 for the two classical signals and the water-filling method.

*3) Resolution:* In order to compare the resolution, CFs of the five abovementioned waveforms are shown in Fig. 10, and their 3-dB mainlobe widths of CF are also listed in Table I.

It can be observed that the proposed schemes for both the LFM signal and P4 sequence have a slight loss in resolution compared with the classical waveforms. It indicates that the joint design can not only help the classical high-resolution radar improve their information acquisition ability but also maintain the high-resolution property well. With the matched filter, the water-filling method has a high resolution. However, it may be a coincidence, as the resolution requirement is not considered there. The waveform designed by the water-filling scheme relies on the PSD of target scattering, clutter, and

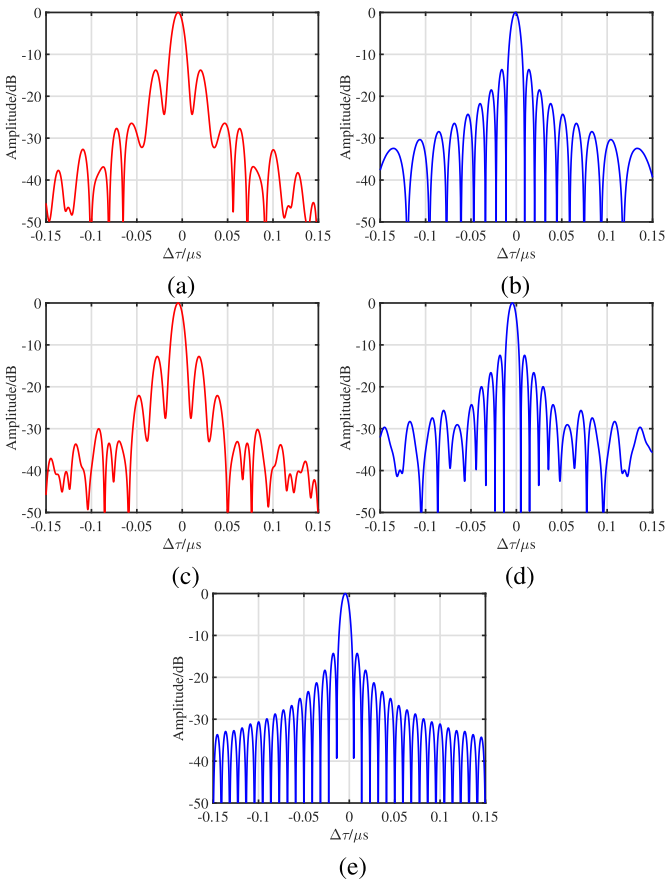


Fig. 10. CFs corresponding to different waveforms: (a) CF of the weighted LFM signal, (b) CF of the classical LFM signal, (c) CF of the weighted P4 sequence, (d) CF of the classical P4 sequence, and (e) CF of the water-filling waveform.

noise [19] so that high resolution cannot always be guaranteed with respect to any shapes of the PSD. Returning to the proposed scheme, its resolution is mainly determined by $\varepsilon_1$ and $\varepsilon_2$, so that high resolution can always be maintained very well.

## V. CONCLUSION

Based on the MTIC, a joint design of transmit weight sequence and optimal filter for high-resolution radar has been presented, to improve target information acquisition and, at the same time, maintain its high-resolution property. The main results can be summarized as follows.

The transmit weight sequence and receive filter design problem for high-resolution radar was formulated as maximizing information acquisition subject to energy and similarity constraints, which resulted in a nonconvex fractional QCQP. Combined with a bivariate auxiliary function based on Dinkelbach's algorithm, a solving method with a polynomial computational complexity was developed by alternately solving two SDR problems, whose convergence was analytically proved. Through a suitable rank-one decomposition, it was confirmed that the optimal solution obtained from the iterative process is also optimal to the original QCQP. Numerical results have shown that the radar with improved design has

achieved better information acquisition and detection performance with a similar resolution compared with the classical high-resolution radar and the widely discussed water-filling method with the matched filter.

## APPENDIX

### A. Proof of the SDR Representation

In this appendix, the SDR formulation of objective function and constraints in (7) are derived, respectively.

*1) Objective Function:*

$$\max_{\mathbf{s},\mathbf{w}} \frac{\mathbf{w}^H\mathbf{T}(\mathbf{s})\mathbf{w}}{\mathbf{w}^H[\mathbf{\Gamma}(\mathbf{s})+\mathbf{R}_V]\mathbf{w}} \rightarrow \max_{\mathbf{X},\mathbf{W}} \frac{\mathrm{tr}\big[\bar{\mathbf{T}}(\mathbf{X})\mathbf{W}\big]}{\mathrm{tr}\big\{\big[\bar{\mathbf{\Gamma}}(\mathbf{X})+\mathbf{R}_V\big]\mathbf{W}\big\}}.$$

The Toeplitz matrix $\mathcal{G}(\ell)$ can be reformulated as

$$\mathcal{G}(\ell) = \sum_{n=-N+1}^{N-1} G(n+\ell)\mathbf{J}_n$$

where $\mathbf{J}_n$ is defined as

$$\mathbf{J}_n(i,j) = \begin{cases} 1, & \text{if } i-j=n \\ 0, & \text{if } i-j\neq n. \end{cases}$$

Assuming that $r_G(\cdot)$ is the autocorrelation function of $G(t)$, $\mathbf{\Gamma}(\mathbf{s})$ in (4) can be recast as

$$\begin{aligned}\mathbf{\Gamma}(\mathbf{s}) &= \mathrm{E}\big[G(\ell+n_1)G^*(\ell+n_2)\big] \\ &\quad\cdot\left(\sum_{n_1=-N+1}^{N-1}\mathbf{J}_{n_1}\right)(\mathbf{s}\odot\mathbf{c})\big(\mathbf{c}^H\odot\mathbf{s}^H\big)\left(\sum_{n_2=-N+1}^{N-1}\mathbf{J}_{n_2}\right)^H \\ &= r_G(n_1-n_2) \\ &\quad\cdot\left(\sum_{n_1=-N+1}^{N-1}\mathbf{J}_{n_1}\right)\big(\mathbf{s}\mathbf{s}^H\big)\odot\big(\mathbf{c}\mathbf{c}^H\big)\left(\sum_{n_2=-N+1}^{N-1}\mathbf{J}_{n_2}\right)^H.\end{aligned} \tag{22}$$

Then, substituting $\mathbf{X}=\mathbf{s}\mathbf{s}^H$ into the expression of $\mathbf{T}(\mathbf{s})$ in (3) and $\mathbf{\Gamma}(\mathbf{s})$ in (22), respectively, $\bar{\mathbf{T}}(\mathbf{X})$ and $\bar{\mathbf{\Gamma}}(\mathbf{X})$ are then obtained.

*2) Constraints:* The energy constraint is easy to prove, so we only consider the similarity constraint. Since $\|\mathbf{s}\odot\mathbf{c}-\mathbf{c}\|^2\le\varepsilon_1$, we obtain

$$\|\mathbf{s}\odot\mathbf{c}-\mathbf{c}\|^2 = 2\|\mathbf{c}\|^2 - 2\,\mathrm{Re}\big[(\mathbf{s}\odot\mathbf{c})^H\mathbf{c}\big] \le \varepsilon_1.$$

It implies that

$$\big\|(\mathbf{s}\odot\mathbf{c})^H\mathbf{c}\big\|^2 \ge \big\{\mathrm{Re}\big[(\mathbf{s}\odot\mathbf{c})^H\mathbf{c}\big]\big\}^2 \ge [(2E_c-\varepsilon_1)/2\,]^2$$

where $\|\mathbf{c}\|^2=E_c$. Moreover, $\|(\mathbf{s}\odot\mathbf{c})^H\mathbf{c}\|^2$ can be reformulated as

$$\begin{aligned}\big\|(\mathbf{s}\odot\mathbf{c})^H\mathbf{c}\big\|^2 &= \mathrm{tr}\Big[\mathbf{s}^H\Big(\mathbf{c}\mathbf{c}^H\odot\big(\mathbf{c}\mathbf{c}^H\big)^*\Big)\mathbf{s}\Big] \\ &= \mathrm{tr}\Big[\Big(\mathbf{c}\mathbf{c}^H\odot\big(\mathbf{c}\mathbf{c}^H\big)^*\Big)\mathbf{X}\Big].\end{aligned}$$

Finally, if

$$\bar{\varepsilon}_1 = [(2E_c-\varepsilon_1)/2\,]^2$$

it is straightforward to verify that

$$\|\mathbf{s}\odot\mathbf{c}-\mathbf{c}\|^2\le\varepsilon_1 \rightarrow \mathrm{tr}\Big[\Big(\mathbf{c}\mathbf{c}^H\odot\big(\mathbf{c}\mathbf{c}^H\big)^*\Big)\mathbf{X}\Big] \ge \bar{\varepsilon}_1.$$

The case of the receive filter can be treated similarly.

### B. Proof of Equation (11)

With $\mathbf{W}^m\in\mathcal{S}(\mathcal{P}_1)$, it leads to

$$\begin{aligned}&\Psi\big(\mathbf{X}^{(m-1)},\mathbf{W}^{(m)};\mathbf{X}^{(m-1)},\mathbf{W}^{(m-1)}\big) \\ &\qquad\ge \Psi\big(\mathbf{X}^{(m-1)},\mathbf{W}^{(m-1)};\mathbf{X}^{(m-1)},\mathbf{W}^{(m-1)}\big).\end{aligned}$$

Since there must exist

$$\begin{aligned}&\Psi\big(\mathbf{X}^{(m-1)},\mathbf{W}^{(m-1)};\mathbf{X}^{(m-1)},\mathbf{W}^{(m-1)}\big) \\ &\quad= \mu\big(\mathbf{X}^{(m-1)},\mathbf{W}^{(m-1)}\big)-\eta\big(\mathbf{X}^{(m-1)},\mathbf{W}^{(m-1)}\big) \\ &\qquad\cdot\bar{f}\big(\mathbf{X}^{(m-1)},\mathbf{W}^{(m-1)}\big)=0\end{aligned}$$

it follows that

$$\begin{aligned}\Psi\big(\mathbf{X}^{(m-1)},\mathbf{W}^{(m)};\mathbf{X}^{(m-1)},\mathbf{W}^{(m-1)}\big) &= \mu\big(\mathbf{X}^{(m-1)},\mathbf{W}^{(m)}\big) \\ &\quad-\eta\big(\mathbf{X}^{(m-1)},\mathbf{W}^{(m)}\big)\cdot\bar{f}\big(\mathbf{X}^{(m-1)},\mathbf{W}^{(m-1)}\big)\ge 0.\end{aligned}$$

Meanwhile,

$$\begin{aligned}\Psi\big(\mathbf{X}^{(m-1)},\mathbf{W}^{(m)};\mathbf{X}^{(m-1)},\mathbf{W}^{(m)}\big) &= \mu\big(\mathbf{X}^{(m-1)},\mathbf{W}^{(m)}\big) \\ &\quad-\eta\big(\mathbf{X}^{(m-1)},\mathbf{W}^{(m)}\big)\cdot\bar{f}\big(\mathbf{X}^{(m-1)},\mathbf{W}^{(m)}\big)=0.\end{aligned}$$

With $\mu(\mathbf{X}^{(m-1)},\mathbf{W}^{(m)})\ge 0$ and $\eta(\mathbf{X}^{(m-1)},\mathbf{W}^{(m)})>0$, we have

$$\bar{f}\big(\mathbf{X}^{(m-1)},\mathbf{W}^{(m)}\big)\ge\bar{f}\big(\mathbf{X}^{(m-1)},\mathbf{W}^{(m-1)}\big).$$

### C. Proof of Equation (15)

The homogenized version of $\mu(\mathbf{X},\mathbf{W})$ in (9) can be written as

$$\begin{aligned}\mu\big(\mathbf{X},\mathbf{W}^{(m)}\big) &= \big(\mathbf{w}^{(m)}\big)^H\bar{\mathbf{T}}(\mathbf{X})\mathbf{w}^{(m)} \\ &= \big(\mathbf{w}^{(m)}\big)^H\mathbf{R}_G\big[(\mathbf{s}\odot\mathbf{c})(\mathbf{s}\odot\mathbf{c})^H\big]\mathbf{R}_G^H\mathbf{w}^{(m)} \\ &= (\mathbf{s}\odot\mathbf{c})^H\mathbf{R}_G^H\mathbf{W}^{(m)}\mathbf{R}_G(\mathbf{s}\odot\mathbf{c}) \\ &= \mathbf{s}^H\Big[\big(\mathbf{c}\mathbf{c}^H\big)^*\odot\big(\mathbf{R}_G^H\mathbf{W}^{(m)}\mathbf{R}_G\big)\Big]\mathbf{s} \\ &= \mathrm{tr}\Big\{\Big[\big(\mathbf{c}\mathbf{c}^H\big)^*\odot\big(\mathbf{R}_G^H\mathbf{W}^{(m)}\mathbf{R}_G\big)\Big]\mathbf{X}\Big\} \\ &= \hat{\mu}\big(\mathbf{X},\mathbf{W}^{(m)}\big).\end{aligned}$$

In a similar way, we obtain

$$\eta\big(\mathbf{X},\mathbf{W}^{(m)}\big)=\hat{\eta}\big(\mathbf{X},\mathbf{W}^{(m)}\big).$$

As a result, (15) is confirmed.

### D. Proof of Lemma 1

Because $\mathcal{V}(\mathcal{P}_1)=\mathcal{V}(\mathcal{P}_2)=0$, there is at least one solution pair $(\mathbf{X}',\mathbf{W}')$, for example, $(\mathbf{X}^{m^*},\mathbf{W}^{m^*})$ such that

$$\mu\big(\mathbf{X}',\mathbf{W}'\big)-\eta\big(\mathbf{X}',\mathbf{W}'\big)\bar{f}\big(\mathbf{X}^\dagger,\mathbf{W}^\dagger\big)=0.$$

Then,

$$\bar{f}\big(\mathbf{X}^\dagger,\mathbf{W}^\dagger\big)=\frac{\mu\big(\mathbf{X}',\mathbf{W}'\big)}{\eta(\mathbf{X}',\mathbf{W}')}.$$

Since $(\mathbf{X}',\mathbf{W}')$ is a feasible solution of problem $\mathcal{P}_{\mathbf{X},\mathbf{W}}$

$$\bar{f}\big(\mathbf{X}^\dagger,\mathbf{W}^\dagger\big)\le\bar{f}(\mathbf{X_0},\mathbf{W}_0)=\frac{\mu(\mathbf{X}_0,\mathbf{W}_0)}{\eta(\mathbf{X}_0,\mathbf{W}_0)}$$

where $(\mathbf{X}_0, \mathbf{W}_0) \in \mathcal{S}(\mathcal{P}_{\mathbf{X},\mathbf{W}})$ is an optimal solution to $\mathcal{P}_{\mathbf{X},\mathbf{W}}$. It follows that

$$\mu(\mathbf{X}_0, \mathbf{W}_0) - \eta(\mathbf{X}_0, \mathbf{W}_0)\bar{f}\left(\mathbf{X}^\dagger, \mathbf{W}^\dagger\right) \geq 0. \tag{23}$$

Then, we define $F^\dagger(\mathbf{X}, \mathbf{W})$ for further derivation, i.e.,

$$F^\dagger(\mathbf{X}, \mathbf{W}) = \mu(\mathbf{X}, \mathbf{W}) - \eta(\mathbf{X}, \mathbf{W})\bar{f}\left(\mathbf{X}^\dagger, \mathbf{W}^\dagger\right).$$

Combined with all constraints of $\mathcal{P}_1$ and $\mathcal{P}_2$, we can formulate another optimization problem $\mathcal{P}_3$

$$\mathcal{P}_3 \begin{cases} \max\limits_{\mathbf{X},\mathbf{W}} \ F^\dagger(\mathbf{X}, \mathbf{W}) \\ \text{s.t.} \begin{cases} \mathbf{X} \in \mathcal{D}_X \\ \mathbf{W} \in \mathcal{D}_W \end{cases} \end{cases}$$

where $\mathcal{D}_X$ and $\mathcal{D}_W$ are the feasible regions corresponding to $\mathcal{P}_2$ and $\mathcal{P}_1$, respectively. As mentioned above, the iterative process converges at the $m^*$th step. At this point, when $\mathbf{X} = \mathbf{X}^{(m^*)}$ is substituted into $\mathcal{P}_3$, $\mathbf{W}^{(m^*+1)}$ can be obtained by solving $\mathcal{P}_1$ or $\mathcal{P}_3$ with respect to $\mathbf{W}$ because these two problems have the same feasible region and objective function, with the conclusion of (19). Similarly, we also obtain $\mathbf{X}^{(m^*+1)}$ after $\mathcal{P}_2$ or $\mathcal{P}_3$ is tackled with $\mathbf{W} = \mathbf{W}^{(m^*+1)}$. Thus, starting from the $m^*$th step, the sequential optimization procedure of $\mathcal{P}_3$ is equivalent to alternately iterating $\mathcal{P}_2$ and $\mathcal{P}_1$, which will form a solution sequence of $\mathcal{P}_3$ by fixing one of the two variables and varying the other. Thus, $F^\dagger(\mathbf{X}^{(m)}, \mathbf{W}^{(m)})$ keeps increasing monotonically [52]

$$\begin{aligned} F^\dagger\left(\mathbf{X}^{(m^*)}, \mathbf{W}^{(m^*)}\right) &\leq F^\dagger\left(\mathbf{X}^{(m^*)}, \mathbf{W}^{(m^*+1)}\right) \\ &\leq F^\dagger\left(\mathbf{X}^{(m^*+1)}, \mathbf{W}^{(m^*+1)}\right). \end{aligned} \tag{24}$$

With (9), it always holds true that

$$\mu\left(\mathbf{X}^{(m^*)}, \mathbf{W}^{(m^*)}\right) - \eta\left(\mathbf{X}^{(m^*)}, \mathbf{W}^{(m^*)}\right) \cdot \bar{f}\left(\mathbf{X}^{(m^*)}, \mathbf{W}^{(m^*)}\right) = 0. \tag{25}$$

By the conclusion of (19), (25) is transformed into

$$\mu\left(\mathbf{X}^{(m^*)}, \mathbf{W}^{(m^*)}\right) - \eta\left(\mathbf{X}^{(m^*)}, \mathbf{W}^{(m^*)}\right) \cdot \bar{f}\left(\mathbf{X}^\dagger, \mathbf{W}^\dagger\right) = 0.$$

Thus, we have $F^\dagger(\mathbf{X}^{(m^*)}, \mathbf{W}^{(m^*)}) = 0$. Similarly, with $\mathcal{V}(\mathcal{P}_1) = \mathcal{V}(\mathcal{P}_2) = 0$, it follows:

$$F^\dagger\left(\mathbf{X}^{(m^*)}, \mathbf{W}^{(m^*+1)}\right) = F^\dagger\left(\mathbf{X}^{(m^*+1)}, \mathbf{W}^{(m^*+1)}\right) = 0$$

which further leads to

$$\begin{aligned} F^\dagger\left(\mathbf{X}^{(m^*)}, \mathbf{W}^{(m^*)}\right) &= F^\dagger\left(\mathbf{X}^{(m^*)}, \mathbf{W}^{(m^*+1)}\right) \\ &= F^\dagger\left(\mathbf{X}^{(m^*+1)}, \mathbf{W}^{(m^*+1)}\right) = 0. \end{aligned}$$

According to (24), $F^\dagger(\mathbf{X}^{(m)}, \mathbf{W}^{(m)})$ is a monotonic increasing sequence with respect to $m$. When it remains stable, $F^\dagger(\mathbf{X}, \mathbf{W})$ will reach the maximum value $F^\dagger(\mathbf{X}^{(m^*+1)}, \mathbf{W}^{(m^*+1)})$. Meanwhile, the objective function $F^\dagger(\mathbf{X}, \mathbf{W})$ of $\mathcal{P}_3$ is a biaffine function, so the optimal solution is obtained at the boundary point. Because all of the constraints of $\mathcal{P}_3$ are affine in both $\mathbf{X}$ and $\mathbf{W}$, and they limit the feasible region to the positive orthant, $F^\dagger(\mathbf{X}, \mathbf{W})$ is monotonic in one of the decision variables when the other one is fixed. Thus, there exists only one maximum, which is the global maximum, and we have

$$\begin{aligned} F^\dagger(\mathbf{X}_0, \mathbf{W}_0) &= \mu(\mathbf{X}_0, \mathbf{W}_0) - \eta(\mathbf{X}_0, \mathbf{W}_0)\bar{f}\left(\mathbf{X}^\dagger, \mathbf{W}^\dagger\right) \\ &\leq F^\dagger\left(\mathbf{X}^{(m^*+1)}, \mathbf{W}^{(m^*+1)}\right) = 0. \end{aligned}$$

Combing (23), then

$$\mu(\mathbf{X}_0, \mathbf{W}_0) - \eta(\mathbf{X}_0, \mathbf{W}_0)\bar{f}\left(\mathbf{X}^\dagger, \mathbf{W}^\dagger\right) = 0.$$

Hence,

$$\begin{aligned} \bar{f}\left(\mathbf{X}^\dagger, \mathbf{W}^\dagger\right) &= \frac{\mu(\mathbf{X}_0, \mathbf{W}_0)}{\eta(\mathbf{X}_0, \mathbf{W}_0)} \\ &= \bar{f}(\mathbf{X}_0, \mathbf{W}_0). \end{aligned}$$

The proof is complete.

## REFERENCES


[1] S. D. Blunt and E. L. Mokole, "Overview of radar waveform diversity," *IEEE Aerosp. Electron. Syst. Mag.*, vol. 31, no. 11, pp. 2–42, Nov. 2016.

[2] C. Tison, J. M. Nicolas, F. Tupin, and H. Maitre, "A new statistical model for Markovian classification of urban areas in high-resolution SAR images," *IEEE Trans. Geosci. Remote Sens.*, vol. 42, no. 10, pp. 2046–2057, Oct. 2004.

[3] H. Lang, Y. Xi, and X. Zhang, "Ship detection in high-resolution SAR images by clustering spatially enhanced pixel descriptor," *IEEE Trans. Geosci. Remote Sens.*, vol. 57, no. 8, pp. 5407–5423, Aug. 2019.

[4] M. Burgos-Garcia, F. Perez-Martinez, and J. G. Menoyo, "Radar signature of a helicopter illuminated by a long LFM signal," *IEEE Trans. Aerosp. Electron. Syst.*, vol. 45, no. 3, pp. 1104–1110, Jul. 2009.

[5] K. Tang, X. Sun, H. Sun, and H. Wang, "A geometrical-based simulator for target recognition in high-resolution SAR images," *IEEE Geosci. Remote Sens. Lett.*, vol. 9, no. 5, pp. 958–962, Sep. 2012.

[6] Y. Sun, Z. Liu, S. Todorovic, and J. Li, "Adaptive boosting for SAR automatic target recognition," *IEEE Trans. Aerosp. Electron. Syst.*, vol. 43, no. 1, pp. 112–125, Jan. 2007.

[7] J. C. Souyris, C. Henry, and F. Adragna, "On the use of complex SAR image spectral analysis for target detection: Assessment of polarimetry," *IEEE Trans. Geosci. Remote Sens.*, vol. 41, no. 12, pp. 2725–2734, Dec. 2003.

[8] W.-Q. Wang, "MIMO SAR OFDM chirp waveform diversity design with random matrix modulation," *IEEE Trans. Geosci. Remote Sens.*, vol. 53, no. 3, pp. 1615–1625, Mar. 2015.

[9] R. M. Beauchamp, S. Tanelli, E. Peral, and V. Chandrasekar, "Pulse compression waveform and filter optimization for spaceborne cloud and precipitation radar," *IEEE Trans. Geosci. Remote Sens.*, vol. 55, no. 2, pp. 915–931, Feb. 2017.

[10] J. R. Klauder, A. C. Price, S. Darlington, and W. J. Albersheim, "The theory and design of chirp radars," *Bell Syst. Tech. J.*, vol. 39, no. 4, pp. 745–808, 1960.

[11] N. Levanon and E. Mozeson, *Radar Signals*. New York, NY, USA: Wiley, 2004, pp. 86–95.

[12] J. Yang, X. Huang, T. Jin, J. Thompson, and Z. Zhou, "Synthetic aperture radar imaging using stepped frequency waveform," *IEEE Trans. Geosci. Remote Sens.*, vol. 50, no. 5, pp. 2026–2036, May 2012.

[13] F. F. Kretschmer, Jr. and K. Gerlach, "Low sidelobe radar waveforms derived from orthogonal matrices," *IEEE Trans. Aerosp. Electron. Syst.*, vol. 27, no. 1, pp. 92–102, Jan. 1991.

[14] P. Stoica, H. He, and J. Li, "New algorithms for designing unimodular sequences with good correlation properties," *IEEE Trans. Signal Process.*, vol. 57, no. 4, pp. 1415–1425, Apr. 2009.

[15] M. A. Kerahroodi, A. Aubry, A. D. Maio, M. M. Naghsh, and M. Modarres-Hashemi, "A coordinate-descent framework to design low PSL/ISL sequences," *IEEE Trans. Signal Process.*, vol. 65, no. 22, pp. 5942–5956, Nov. 2017.

[16] M. Alaee-Kerahroodi, M. Modarres-Hashemi, and M. M. Naghsh, "Designing sets of binary sequences for MIMO radar systems," *IEEE Trans. Signal Process.*, vol. 67, no. 13, pp. 3347–3360, Jul. 2019.

[17] S. Sen, "PAPR-constrained Pareto-optimal waveform design for OFDM-STAP radar," *IEEE Trans. Geosci. Remote Sens.*, vol. 52, no. 6, pp. 3658–3669, Jun. 2014.

[18] P. M. Woodward, *Probability and Information Theory With Applications to Radar*, 2nd ed. London, U.K.: Pergamon, 1964, pp. 62–80.

[19] M. R. Bell, "Information theory and radar waveform design," *IEEE Trans. Inf. Theory*, vol. 39, no. 5, pp. 1578–1597, Sep. 1993.

[20] G. Dong and G. Kuang, "Classification on the monogenic scale space: Application to target recognition in SAR image," *IEEE Trans. Image Process.*, vol. 24, no. 8, pp. 2527–2539, Aug. 2015.

[21] K. El-Darymli, E. W. Gill, P. Mcguire, D. Power, and C. Moloney, "Automatic target recognition in synthetic aperture radar imagery: A state-of-the-art review," *IEEE Access*, vol. 4, pp. 6014–6058, 2016.

[22] H. Estephan, M. G. Amin, and K. M. Yemelyanov, "Optimal waveform design for improved indoor target detection in sensing through-the-wall applications," *IEEE Trans. Geosci. Remote Sens.*, vol. 48, no. 7, pp. 2930–2941, Jul. 2010.

[23] Y. Gu and N. A. Goodman, "Information-theoretic waveform design for Gaussian mixture radar target profiling," *IEEE Trans. Aerosp. Electron. Syst.*, vol. 55, no. 3, pp. 1528–1536, Jun. 2019.

[24] A. Leshem, O. Naparstek, and A. Nehorai, "Information theoretic adaptive radar waveform design for multiple extended targets," *IEEE J. Sel. Topics Signal Process.*, vol. 1, no. 1, pp. 42–55, Jun. 2007.

[25] R. A. Romero, J. Bae, and N. A. Goodman, "Theory and application of SNR and mutual information matched illumination waveforms," *IEEE Trans. Aerosp. Electron. Syst.*, vol. 47, no. 2, pp. 912–927, Apr. 2011.

[26] Y. Yang and R. S. Blum, "MIMO radar waveform design based on mutual information and minimum mean-square error estimation," *IEEE Trans. Aerosp. Electron. Syst.*, vol. 43, no. 1, pp. 330–343, Jan. 2007.

[27] B. Tang, J. Tang, and Y. Peng, "MIMO radar waveform design in colored noise based on information theory," *IEEE Trans. Signal Process.*, vol. 58, no. 9, pp. 4684–4697, Sep. 2010.

[28] N. A. Goodman, P. R. Venkata, and M. A. Neifeld, "Adaptive waveform design and sequential hypothesis testing for target recognition with active sensors," *IEEE J. Sel. Topics Signal Process.*, vol. 1, no. 1, pp. 105–113, Jun. 2007.

[29] G. Sun, Z. He, J. Tong, X. Yu, and S. Shi, "Mutual information-based waveform design for MIMO radar space-time adaptive processing," *IEEE Trans. Geosci. Remote Sens.*, vol. 59, no. 4, pp. 2909–2921, Apr. 2021.

[30] Z. Zhu, S. Kay, and R. S. Raghavan, "Information-theoretic optimal radar waveform design," *IEEE Signal Process. Lett.*, vol. 24, no. 3, pp. 274–278, Mar. 2017.

[31] Y. Chen, Y. Nijsure, C. Yuen, Y. H. Chew, Z. Ding, and S. Boussakta, "Adaptive distributed MIMO radar waveform optimization based on mutual information," *IEEE Trans. Aerosp. Electron. Syst.*, vol. 49, no. 2, pp. 1374–1385, Apr. 2013.

[32] A. Aubry, A. DeMaio, A. Farina, and M. Wicks, "Knowledge-aided (potentially cognitive) transmit signal and receive filter design in signal-dependent clutter," *IEEE Trans. Aerosp. Electron. Syst.*, vol. 49, no. 1, pp. 93–117, Jan. 2013.

[33] Y. Huang, L. Zhang, J. Li, Z. Chen, and X. Yang, "Reweighted tensor factorization method for SAR narrowband and wideband interference mitigation using smoothing multiview tensor model," *IEEE Trans. Geosci. Remote Sens.*, vol. 58, no. 5, pp. 3298–3313, May 2020.

[34] Y. Huang *et al.*, "An efficient graph-based algorithm for time-varying narrowband interference suppression on SAR system," *IEEE Trans. Geosci. Remote Sens.*, early access, Feb. 1, 2021, doi: 10.1109/TGRS.2021.3051192.

[35] A. M. Ahmed, A. Alameer, D. Erni, and A. Sezgin, "Maximizing information extraction of extended radar targets through MIMO beamforming," *IEEE Geosci. Remote Sens. Lett.*, vol. 16, no. 4, pp. 539–543, Apr. 2019.

[36] V. S. Frost and K. S. Shanmugan, "The information content of synthetic aperture radar images of terrain," *IEEE Trans. Aerosp. Electron. Syst.*, vol. AES-19, no. 5, pp. 768–774, Sep. 1983.

[37] S. Z. Alshirah, S. Gishkori, and B. Mulgrew, "Frequency-based optimal radar waveform design for classification performance maximization using multiclass Fisher analysis," *IEEE Trans. Geosci. Remote Sens.*, vol. 59, no. 4, pp. 3010–3021, Apr. 2021.

[38] X. Zeng and T. S. Durrani, "Estimation of mutual information using copula density function," *Electron. Lett.*, vol. 47, no. 8, pp. 493–494, Apr. 2011.

[39] S. D. Blunt and K. Gerlach, "Adaptive pulse compression via MMSE estimation," *IEEE Trans. Aerosp. Electron. Syst.*, vol. 42, no. 2, pp. 572–584, Apr. 2006.

[40] A. D. Maio, S. D. Nicola, Y. Huang, S. Zhang, and A. Farina, "Code design to optimize radar detection performance under accuracy and similarity constraints," *IEEE Trans. Signal Process.*, vol. 56, no. 11, pp. 5618–5629, Nov. 2008.

[41] A. D. Maio, S. D. Nicola, Y. Huang, Z. Q. Luo, and S. Zhang, "Design of phase codes for radar performance optimization with a similarity constraint," *IEEE Trans. Signal Process.*, vol. 57, no. 2, pp. 610–621, Feb. 2009.

[42] I. M. Stancu-Minasian, *Fractional Programming: Theory, Methods and Applications*. Norwell, MA, USA: Kluwer, 1992, pp. 133–159.

[43] A. De Maio, Y. Huang, D. P. Palomar, S. Zhang, and A. Farina, "Fractional QCQP with applications in ML steering direction estimation for radar detection," *IEEE Trans. Signal Process.*, vol. 59, no. 1, pp. 172–185, Jan. 2011.

[44] A. B. Gershman, N. D. Sidiropoulos, S. Shahbazpanahi, M. Bengtsson, and B. Ottersten, "Convex optimization-based beamforming," *IEEE Signal Process. Mag.*, vol. 27, no. 3, pp. 62–75, May 2010.

[45] M. M. Naghsh, M. Soltanalian, P. Stoica, M. Modarres-Hashemi, A. De Maio, and A. Aubry, "A Doppler robust design of transmit sequence and receive filter in the presence of signal-dependent interference," *IEEE Trans. Signal Process.*, vol. 62, no. 4, pp. 772–785, Feb. 2014.

[46] S. M. Karbasi, A. Aubry, A. D. Maio, and M. H. Bastani, "Robust transmit code and receive filter design for extended targets in clutter," *IEEE Trans. Signal Process.*, vol. 63, no. 8, pp. 1965–1976, Apr. 2015.

[47] W. Fan, J. Liang, and J. Li, "Constant modulus MIMO radar waveform design with minimum peak sidelobe transmit beampattern," *IEEE Trans. Signal Process.*, vol. 66, no. 16, pp. 4207–4222, Aug. 2018.

[48] W. Dinkelbach, "On nonlinear fractional programming," *Manage. Sci.*, vol. 13, no. 7, pp. 492–498, Mar. 1967.

[49] J. Lofberg, "YALMIP: A toolbox for modeling and optimization in MATLAB," in *Proc. IEEE Int. Conf. Robot. Autom.*, Sep. 2004, pp. 284–289.

[50] W. Ai, Y. Huang, and S. Zhang, "New results on Hermitian matrix rank-one decomposition," *Math. Program.*, vol. 128, nos. 1–2, pp. 253–283, Jun. 2011.

[51] B. Tang and J. Li, "Spectrally constrained MIMO radar waveform design based on mutual information," *IEEE Trans. Signal Process.*, vol. 67, no. 3, pp. 821–834, Feb. 2019.

[52] P. Stoica and Y. Selén, "Cyclic minimizers, majorization techniques, and the expectation-maximization algorithm: A refresher," *IEEE Signal Process. Mag.*, vol. 21, no. 1, pp. 112–114, Jan. 2004.


**Jiawei Zhang** (Graduate Student Member, IEEE) received the B.S. and M.S. degrees in electronic engineering from Yanshan University, Qinhuangdao, China, in 2014 and 2017, respectively. He is pursuing the Ph.D. degree with the School of Electronic and Information Engineering, Beihang University, Beijing, China.

His research interests are in radar waveform design and signal processing for synthetic aperture radar.

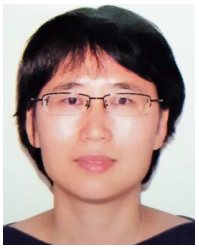

**Huaping Xu** (Member, IEEE) received the B.S. degree in electronic engineering and the Ph.D. degree in communication and information systems from Beihang University, Beijing, China, in 1998 and 2003, respectively.

She is a Professor with the School of Electronic and Information Engineering, Beihang University. She has now published more than 100 journal articles and conference papers and a research monograph about signal processing. Her research interests include synthetic aperture radar (SAR) interferometry, differential SAR interferometry, image processing, and radar waveform design.

**Wei Liu** (Senior Member, IEEE) received the B.Sc. and L.L.B. degrees from Peking University, Beijing, China, in 1996 and 1997, respectively, the M.Phil. degree from The University of Hong Kong, Hong Kong, in 2001, and the Ph.D. degree from the School of Electronics and Computer Science, University of Southampton, Southampton, U.K., in 2003.

He held a post-doctoral position at the University of Southampton and later at the Department of Electrical and Electronic Engineering, Imperial College London, London, U.K. Since September 2005, he has been with the Department of Electronic and Electrical Engineering, The University of Sheffield, Sheffield, U.K., first as a Lecturer and then a Senior Lecturer. He has published about 350 journal articles and conference papers, five book chapters, and two research monographs titled "Wideband Beamforming: Concepts and Techniques" (John Wiley, March 2010) and "Low-Cost Smart Antennas" (Wiley-IEEE, March 2019), respectively. His research interests cover a wide range of topics in signal processing, with a focus on sensor array signal processing and its various applications, such as robotics and autonomous systems, human–computer interface, radar, sonar, satellite navigation, and wireless communications.

Dr. Liu is also a member of the Digital Signal Processing Technical Committee of the IEEE Circuits and Systems Society (Secretary from May 2020) and the Sensor Array and Multichannel Signal Processing Technical Committee of the IEEE Signal Processing Society (Chair from Jan. 2021). He is an Editorial Board Member of the journal *Frontiers of Information Technology and Electronic Engineering* and the *Journal of The Franklin Institute*. He was an Associate Editor of IEEE TRANSACTIONS ON SIGNAL PROCESSING from 2015 to 2019 and IEEE ACCESS from 2016 to 2021.

**Chunsheng Li** received the Ph.D. degree in signal and information processing from Beihang University, Beijing, China, in 1998.

Since 2005, he was a Professor with the School of Electronics and Information Engineering, Beihang University. He has authored more than 100 journal articles and conference papers and four books. His research interests include analysis and simulation of synthetic aperture radar (SAR) satellites, high-resolution image formation, and multimodal remote sensing data fusion.

**Yifan Chen** (Senior Member, IEEE) has held various academic and leadership positions in the universities in China, New Zealand, the U.K., and Singapore. His research interests include computational nanobiosensing where information and communications technologies meet nanomedicines, electromagnetic medical imaging and sensing, and wearable health.